

University of Nebraska - Lincoln

DigitalCommons@University of Nebraska - Lincoln

Mechanical (and Materials) Engineering --
Dissertations, Theses, and Student Research

Mechanical & Materials Engineering,
Department of


Summer 8-2-2013

Measurement and Description of Dynamics Required for *in vivo* Surgical Robotics via Kinematic Methods

Jacob G. Greenburg

University of Nebraska-Lincoln, jgreenb8@gmail.com

Follow this and additional works at: <https://digitalcommons.unl.edu/mechengdiss>

 Part of the [Applied Mechanics Commons](#), [Biomechanical Engineering Commons](#), [Computer-Aided Engineering and Design Commons](#), [Electro-Mechanical Systems Commons](#), [Equipment and Supplies Commons](#), [Investigative Techniques Commons](#), and the [Surgical Procedures, Operative Commons](#)

Greenburg, Jacob G., "Measurement and Description of Dynamics Required for *in vivo* Surgical Robotics via Kinematic Methods" (2013). *Mechanical (and Materials) Engineering -- Dissertations, Theses, and Student Research*. 54.

<https://digitalcommons.unl.edu/mechengdiss/54>

This Article is brought to you for free and open access by the Mechanical & Materials Engineering, Department of at DigitalCommons@University of Nebraska - Lincoln. It has been accepted for inclusion in Mechanical (and Materials) Engineering -- Dissertations, Theses, and Student Research by an authorized administrator of DigitalCommons@University of Nebraska - Lincoln.

MEASUREMENT AND DESCRIPTION OF DYNAMICS REQUIRED FOR *IN VIVO*
SURGICAL ROBOTICS VIA KINEMATIC METHODS

by

Jacob G. Greenburg

A THESIS

Presented to the Faculty of
The Graduate College at the University of Nebraska
In Partial Fulfillment of Requirements
For the Degree of Master of Science

Major: Mechanical Engineering and Applied Mechanics

Under the Supervision of Professor Shane M. Farritor

Lincoln, Nebraska

August, 2013

MEASUREMENT AND DESCRIPTION OF DYNAMICS REQUIRED FOR *IN VIVO* SURGICAL ROBOTICS VIA KINEMATIC METHODS

Jacob Gene Greenburg, M.S.

University of Nebraska, 2013

Advisor: Shane M. Farritor

With the goal of improved recovery times and reduced trauma to the patient there has been a substantial shift in the medical community's demand for minimally invasive surgical (MIS) techniques. With the standardization of MIS becoming more commonplace in the medical field there are still many improvements that are desired. Traditional, manual methods of these surgeries require multiple incisions on the abdomen for the tools and instruments to be inserted. The more recent demand has been to localize the incisions into what is being referred to as a Laparoendoscopic Single-Site (LESS) surgery. Furthermore, the manual instruments that are commonly used are rigid and when inserted create a pivot point with the abdominal wall. The pivot created greatly decreases the intuitiveness and usability of instruments by inverting the required maneuvers of the surgeon. The solution to these problems is to utilize a controlled surgical robotic system designed and optimized for the LESS surgical constraints.

Such a solution recovers normal movement to the surgeon; however, the primary limitation to this answer is the unknown requirements on the design. Although the size of the abdominal cavity and space requirements are fundamentally known by observation, in order to successfully complete a MIS the forces and torques involved are also necessary. Such an observation is much more difficult to obtain and these quantities remain largely unknown. It is the method of acquisition and the discovered magnitude of these that will

be presented in this thesis. It is then possible to utilize these new data to adjust the various parameters of the surgical robot to further optimize abdominal cavity constraint usage.

First,

*To my always supportive wife for her infinite
patience and encouragement*

Second,

To my parents for teaching me to learn

Third,

*To Dr. Shane Farritor and company for the
opportunity and their continued support*

Table of Contents

List of Figures	vii
List of Tables	viii
Chapter 1 Introduction	1
Chapter 2 Background	4
2.1. Minimally Invasive Surgery	4
2.1.1. Laparoscopic Surgery	4
2.1.2. Laparoendoscopic Single-Site Surgery	4
2.1.3. Natural Orifice Transluminal Endoscopic Surgery	5
2.2. Instruments for MIS	5
2.1.4. Traditional Tools.....	5
2.1.5. Quantifying MIS Force and Torque Requirements.....	7
2.3. Robotic Surgery.....	8
2.1.6. Surgical Robotics	8
2.1.7. <i>In Vivo</i> Robotics.....	10
Chapter 3 Motivations for Force and Torque Measurements	12
2.4. <i>In Vivo</i> Robot Concepts.....	12
3.1.1. Manipulability Goals	12
3.1.2. Robotic Platform.....	12
2.5. Measurement Methods	13
3.1.3. Multi-axis Sensor Selection	13
3.1.4. Utilizing Multi-axis Measurement	14
2.6. Design Restraints	15
3.1.5. Robotic Workspace Preservation	15
Chapter 4 Design and methods	17
2.7. Tyler-Bot 2.0.....	17
4.1.1. Kinematic Design.....	17
4.1.2. TB2.0 Denavit-Hartenberg Parameters.....	18
4.1.3. Workspace.....	19

4.1.4. Final Design	20
2.8. Jacob-Tyler-Bot 1.0	24
2.9. Jacob-Tyler-Bot 2.0	27
2.10. Physical Description	31
4.1.5. System Coordinate Frames	32
4.1.6. JTB2.0 Denavit-Hartenberg Parameters	34
4.1.7. Gravitational Analysis	34
2.11. Mathematic Derivations	36
4.1.8. Static Analysis	37
4.1.9. Kinematic Analysis	39
4.1.10. Quasi-Static Derivation.....	40
Chapter 5 Experiments.....	43
2.12. Benchtop Experiments.....	43
5.1.1. Alignment Protocol.....	43
5.1.2. Measurement Verification.....	44
2.13. Surgical Trials	44
Chapter 6 Experimental Results.....	46
2.14. Benchtop Experiments.....	46
2.15. Surgical Trial Data and Discussion.....	50
2.16. Mathematical Analysis.....	55
2.17. Validation	57
Chapter 7 Summary and Conclusions.....	59
References.....	i
Appendix A. Quasi-static scripts.	iv

List of Figures

Figure 1.1. (a) Standard open surgery. (b) MIS with a few incisions. (c) LESS with single incision. (d) NOTES with natural orificies used.	2
Figure 2.1: Standard laparoscopic tools utilized in MIS. [23]	6
Figure 2.2. Intuitive Surgical Inc.'s da Vinci Si [®] [27].	9
Figure 2.3. Overview of the TB2.0 prior to enhancement.	11
Figure 4.1. Reference frame illustration for TB2.0 [29]	18
Figure 4.2. TB2.0 workspace modeled beside human large intestine. [29]	20
Figure 4.3. Illustration of TB2.0. [29].	21
Figure 4.4. TB2.0 Drive train. [29]	22
Figure 4.5. TB2.0's available degrees of freedom. [29]	23
Figure 4.6. TB2.0 configuration prior to modification. [29].	24
Figure 4.7. Side view of the ATI-ia multi-axis sensor. [30]	25
Figure 4.8. Metal mount that converts TB2.0 to the sensor based JTB1.0.	26
Figure 4.9. Assembled left arm of the JTB1.0 prototype.	26
Figure 4.10. JTB2.0 featuring a sensor parallel to the insertion rod.	27
Figure 4.11. Left, TB2.0's original assembly rod; Right, JTB2.0's modified assembly rod.	28
Figure 4.12. Cup interface between multi-axis sensor and insertion rod.	29
Figure 4.13. Left, original torso housing; Right, modified torso housing.	30
Figure 4.14. Final configuration of JTB2.0.	31
Figure 4.15. Side by side comparison of actual and simulated robot.	32
Figure 4.16. New coordinate frame of JTB2.0 in the home position.	33
Figure 4.17. Center of mass for the upper arm of JTB2.0.	35
Figure 4.18. Static free body diagram of JTB2.0.	38
Figure 5.1. Open surgery used to protect equipment.	45
Figure 6.1. Force readings from no load benchtop test.	46
Figure 6.2. Moment readings from no load benchtop test.	47
Figure 6.3. Measured forces when moving with a 250 gram load.	48
Figure 6.4. Measured moments when moving with 250 gram load.	49
Figure 6.5. Raw surgical force data of a robot assisted colectomy.	50
Figure 6.6. Raw surgical moment data of a robot assisted colectomy.	51
Figure 6.7. Top: left, initial grasp; right, stretching for cut. Bottom: left, arms incision; right, inspection.	52
Figure 6.8. Forces measured during a lift and stretch procedure.	53
Figure 6.9. Moments measured during a lift and stretch procedure.	54
Figure 6.10. Force map after rotation and gravity compensation.	56
Figure 6.11. Moment map after rotation and gravity compensation.	57

List of Tables

Table 3.1: BlueDRAGON surgical force measurements.	13
Table 3.2. ATI-IA Nano25 Specifications with US-25-25 Calibration.	14
Table 4.1. TB2.0 DH Parameters and joint limits.	19
Table 4.2. Comparison of DH parameters for TB2.0 and JTB2.0.	34
Table 4.3. Coordinates for the centers of mass.	36
Table 4.4. Simulated mass and weight of each joint of JTB2.0.	36
Table 6.1. Statistical analysis of no load benchtop test.	47
Table 6.2. Statistical analysis of forces in trial #2.	49
Table 6.3. BlueDRAGON surgical force measurements.	58

Chapter 1 Introduction

Since early times, surgical procedures were usually done by opening a large incision in the patient, performing the operation, and experiencing a long recovery time. This was effective and provided the surgeon with much more dexterity and visual ability but was often considered to cause unnecessary trauma to the patient. This trauma typically led to increased recovery times, infection, mortality rates, and cost. Despite the advantages of dexterity provided to the surgeon, the recognition of these drawbacks to the patient made it necessary to seek a better surgical solution.

One such solution was to preform operations using minimally invasive surgery (MIS). With MIS it was now possible to perform procedures with only a few small incisions around the desired site, solving many of the problems of conventional surgery [1]. Through the small openings the surgeon was able to insert laparoscopic tools and other devices into the patient and effectively conduct the surgery [2]. However, as with any new technology problems began to arise. With a long tool inserted into a single incision a pivot point was created due to the interaction with the patient's dermal layers acting as a fulcrum. This made adaptation of MIS slow due to the need to retrain surgeons in order to accept the new inverse coordinate systems (e.g., left is now right, up is now down, and vice versa). As with any good technique further refinement was needed as questions of usability and further reduction of trauma were discussed [3, 4].

In an attempt to answer the increasing question of trauma reduction a new method was developed known as Natural Orifice Translumenal Endoscopic Surgery (NOTES). This method would allow surgeons to access the procedure's site without the use of any

external incisions. NOTES would instead use the natural anatomy of the patient by utilizing natural orifices to gain access [5]. In theory this would address many of the challenges posed by convention surgery by greatly reduce recovery times, increasing cosmetics, and decreasing chance of infection. It also has been found to have significant technological boundaries that need to be addressed, and a large gap was identified between MIS and NOTES [6].

One proposed step between MIS and NOTES was to use a hybrid of the two techniques and utilize a single small incision site through which tools and devices can be inserted. This method became known as Laparoendoscopic Single-Site Surgery (LESS). LESS mimicked NOTES in that the tools had a single entry point but allowed for much of the same tools that MIS utilized [7, 8, 9, 10]. This also led to the same inverse coordinate system problems that MIS faced when using the tools as well as other complications [10, 11, 12, 13]. A comparison of the four types of surgery sites can be found in Figure 1.1 giving a view of the types of incisions each method would require on the torso of the patient.

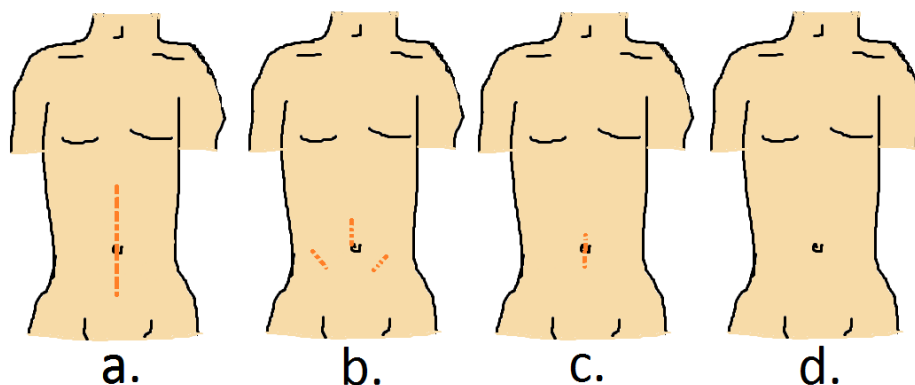


Figure 1.1. (a) Standard open surgery. (b) MIS with a few incisions. (c) LESS with single incision. (d) NOTES with natural orificies used.

Further investigation to the problem led to the use of robotics in the surgical setting [14, 15, 16, 17, 18, 19, 20]. Robotic systems have previously been utilized in MIS methods but still lacked the capabilities of a LESS setting. In order to accommodate LESS and the future of NOTES a new type of completely *in vivo* surgical robotic platform was developed [21]. Utilizing LESS the robotic platform would be fully inserted into an insufflated abdominal cavity and the surgeon would operate via electronic communication. These devices have significant advantages over standard laparoscopic tools by allowing the surgeon to retain the standard hand coordinate system allowing for learned hand movements to be used. The intuitiveness of the system is exemplified by the enhancements that can be virtually applied to the robotic system. Such enhancements can include scaling of the workspace and tremor reduction [22].

Although some of these methods have been successfully used and explored, there still remains an uncertainty in optimizing their design. Only a few observations have been made of the forces and torques required to complete a surgery and fewer still (if any) observations have been made by use of a surgical robotic system. Such a system could provide a study that would give engineers and designers of medical robots further information on the constraints of the surgical system. This information would allow further minimization and optimization of devices that feature a wider range of capabilities.

Chapter 2 Background

2.1. Minimally Invasive Surgery

2.1.1. Laparoscopic Surgery

In recent decades there has been a paradigm shift in the way surgery has been performed. Instead of an open site with a long incision there has been a movement to laparoscopic operations that utilize a new set of tools and a less invasive approach. Minimally invasive surgery (MIS) and laparoscopic procedures have gained momentum and have expanded into many disciplines of medicine as technology and technique have enhanced over the decades since its inception [1]. This is primarily due to the advantages that it poses to patients in reduced cost and increased health benefits [3]. Due to the effectiveness of the technique many surgeries and biomedical engineers alike seek new and novel ways to reduce patient trauma and decrease recovery times by ever decreasing incision size and quantity.

2.1.2. Laparoendoscopic Single-Site Surgery

Laparoendoscopic Single-Site Surgery (LESS) has been considered to be one of the next steps for MIS and has gained popularity despite its inherent increase in difficulty to perform [11]. LESS is similar to MIS in that it reduces the invasiveness of a standard open procedure but instead of multiple small incisions uses a single small incision usually located at the patient's navel. The difficulties of LESS are similar to those of MIS but are amplified by using only a single incision. The surgeon now has to operate in a mirrored manner as well as an inverse coordinate system environment (e.g., left hand is right tool, right hand is left tool, up is down, left is right.). Despite these difficulties it has been documented that performing certain common procedures in this manner can significantly

improve surgical outcomes [7]. With the implementation of LESS there has been a further study into the effects of any incision and questions of further reduction have been posed.

2.1.3. Natural Orifice Translumenal Endoscopic Surgery

Natural Orifice Translumenal Endoscopic Surgery (NOTES) is commonly considered to be a very tantalizing end goal for MIS. Unlike MIS and LESS, NOTES leaves no external scarring as there is no incision involved at the patient's epidermis. This is achieved by accessing the surgical site through more natural means of entrance to the human body, namely the digestive tract. The capabilities of NOTES have been demonstrated in several studies with surviving animal studies and some preliminary results on human studies [5, 6]. This method is widely viewed as the natural next step to MIS; however, given the current state of technology this method is still very difficult to perform. The technology that would be involved is beyond the scope of this document and should be considered for future review and research.

2.2. Instruments for MIS

2.1.4. Traditional Tools

Traditionally, laparoscopic tools used for MIS are long cylindrical devices of different lengths and thicknesses. The tools feature a wide range of graspers, hooks, staplers, and various cutting instruments. An example of the laparoscopic instruments used is shown in Figure 2.1.

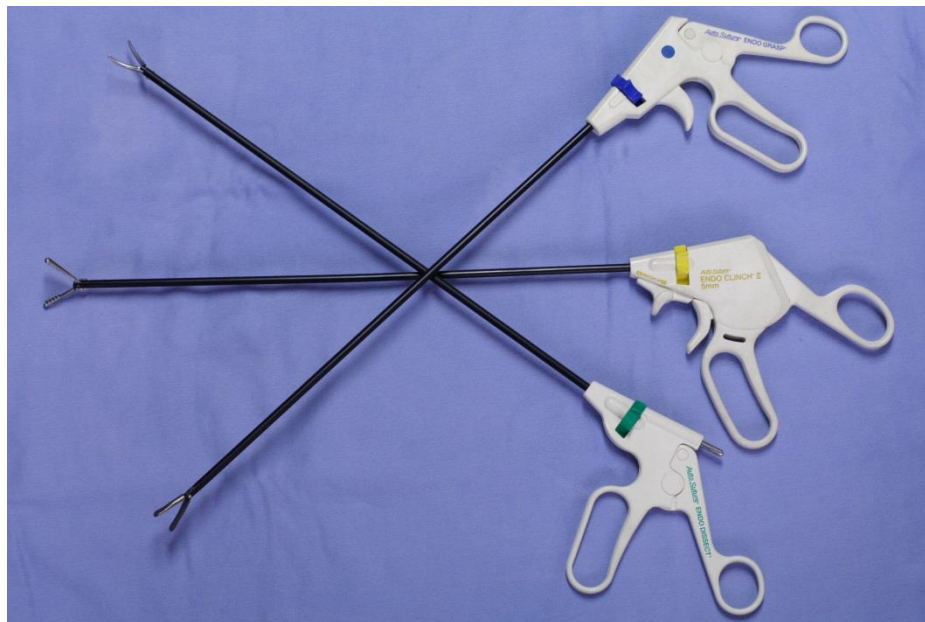


Figure 2.1: Standard laparoscopic tools utilized in MIS. [23]

These tools are generally inserted into a trocar port that has been inserted into the dermis of the patient via a small incision. Such techniques have been highly refined over the years and many tools have become commonplace in the operating room. With many of the same features the tools used for LESS are generally the same ones utilized for MIS. They feature rigid rods with a handle and trigger to operate the grasping end of the tool or other necessary equipment. The largest disadvantage to such tools is the interaction of the rigid rod and the pivot point created at the incision point. This interaction inverts the entire work environment, thus requiring the surgeon to have specialized training and qualifications above standard surgery.

The future of MIS tools would have to be adaptable to be used in a NOTES procedure. Such adaptability could include flexible tools that can be reconfigured in terms of shape or size. These flexible tools would provide the surgeon unprecedented

access to the surgical site. Other tools could also be developed that are considered mechanically separated from the surgeon and are instead ingested into the patient's system. These tools could be controlled via wireless communications and be robotic in nature.

2.1.5. Quantifying MIS Force and Torque Requirements

There have been very few attempts by engineers to quantify the forces and torques required to perform MIS procedures. The most notable of attempts were performed by Rosen *et al.* and K. ikuta *et al.* where an operation was performed using standard laparoscopic tools with a non-intrusive apparatus attached [24, 25]. The kinematics of the apparatus was solved and the position as well as forces and torques were measured. Other attempts at measurement of the necessary forces to lift a section of the colon were performed. One study attempted to quantify the required forces via clamping onto the colon of the subject and using a spring-mass system for measurement. [26]

Such attempts have provided rudimentary information as to what is required of a robotic system to perform various operations. These studies were in fact used as a guideline to produce the robotic system that will be used as a basic platform for this study. Although the studies provided a robust design that was capable for a few procedures, further optimization and verification are warranted to produce a more efficient design.

2.3. Robotic Surgery

2.1.6. Surgical Robotics

More efficient surgical methods have been a topic of interest within the medical communities for some time. Having been provided with many of the issues that currently trouble surgeons and patients alike in MIS, engineers have taken to the challenge of efficiency through design. In the last few decades there has been an apparent observable link between usability and the utility of robotics. Thus, it was natural progression for the engineering and surgical communities to come together and create a new system and yield the field of biomedical device design. With the expertise and knowledge of both medical and engineering fields it was then possible to take a fundamental look towards surgical robotic systems.

Systems that were developed could aid surgeons through a virtual and dynamic control environment that holds ties to the software and electrical aspect of modern science. Such virtual improvements could lead to more precise surgeries via reduced tremor control and scaled movements in hand based operations. Furthermore, these technologies would allow surgery by wire, a new method of intermixing doctors with their patients by allowing them to be miles apart. The previous suggestions on applications are just a beginning; as natural progression of technology occurs much more fantastical ideas can be introduced.

One of the earliest of the surgical robots to be introduced and approved was one produced by Intuitive Surgical, Inc. known as the da Vinci[®] Surgical System. The system was the first of its kind to introduce techniques of MIS into a more natural control

method. The model called da Vinci[®] Si, shown in Figure 2.2, is the latest in MIS surgical robots that are commercially available.



Figure 2.2. Intuitive Surgical Inc.'s da Vinci Si[®] [27].

For all the advancements that the da Vinci[®] brings to the surgical setting, it still has a few features that could be expanded upon and improved. Such items include the size of the device, surgeon comfort, the access and price of the equipment, and virtual enhancements [28]. As for the size of the device, the proposed *in vivo* robotic system would be of the scale to fit within the patient's incision. This provides distinct advantages of internal actuation as opposed to external actuation of previous devices. At this size the equipment would generally be much more cost effective and more readily available. Since both systems feature a surgery by wire approach there are countless possibilities for

virtual enhancement of the surgeon's movements and view of the procedure site.

Furthermore, an *in vivo* system would have the benefit of being expanded to the NOTES surgical scene.

2.1.7. *In Vivo* Robotics

The proposed *in vivo* system would be inserted into the patient's abdominal cavity through a LESS approach. This differs from other approaches by the fact that the robot's actuators would be internal to the patient as opposed to a large external actuation system. Having the robot more localized allows for more precise and easier gross positioning and rearrangement of the surgical site. Instead of new incisions being made to move the patient and the system, the robot can be moved and rotated about a constant single incision. This technique is both a benefit to the patient and the surgeons as it reduces time and trauma in the operating room.

Many systems have been developed at the University of Nebraska Advanced Surgical Technologies Group that can be used for both LESS and NOTES type procedures. Prior research has developed robotics that can be used inside the abdominal cavity for imaging as well as basic surgical tasks [21]. Further, recent research has been done to move towards a more dexterous system that features two multiple use and capable arms. One system that has recently been developed and successfully tested is the Tylerbot 2.0 (TB2.0) as pictured in Figure 2.3 [22]. This system provides the dexterity of surgeon's hands through emulation of multiple degrees of freedom and advanced control systems.

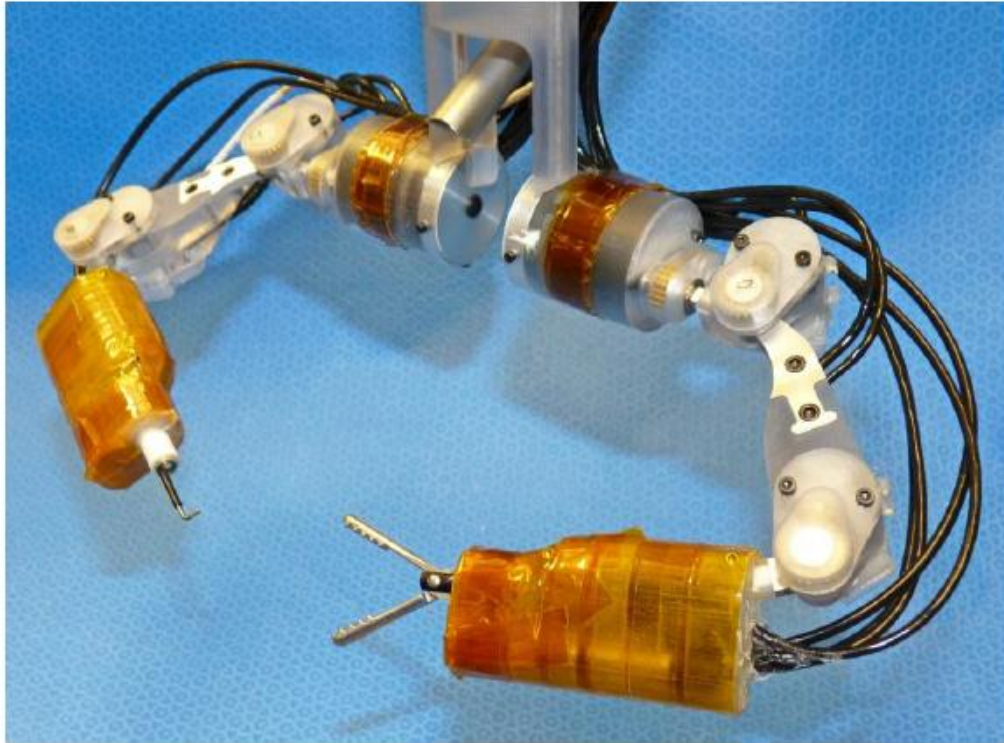


Figure 2.3. Overview of the TB2.0 prior to enhancement.

As these technologies have been developed and tested in previous and ongoing research, it has become apparent that design and reliability has room for optimization. In order to do a complete look at an optimal system, a review of the required dynamics of a surgery was needed. The adaptation and interchangeability of the TB2.0 platform to acquire scientific data will be discussed and analyzed in the following chapters.

Chapter 3 Motivations for Force and Torque Measurements

2.4. *In Vivo* Robot Concepts

3.1.1. Manipulability Goals

In vivo surgical robots are designed with the goal of replacing standard MIS tools and instruments during a surgical procedure. Many of the drawbacks to using a rigid tool are solved when switching to an actuating robotic platform. The robotic platform must be adjustable and dexterous enough to cover the entire work site of the procedure while providing the same movements as a surgeon. Therefore, it has been decided that the best configuration for such a robot would be one that features two arm linkages. Using this linkage system it would be possible to regain two degrees of freedom lost by the pivot point interaction created from the abdominal wall and the standard MIS tools. It is also possible to increase the manipulability of the instrument by the addition of redundant degrees of freedom.

3.1.2. Robotic Platform

In order to meet the requirements of a LESS procedure, the robotic instruments diameter must be small enough to fit in a standard single incision. The generally accepted diameter for such an incision is usually no more than 30 mm. At this size it then becomes difficult to produce a single two-arm system as described above that allows for single insertion type protocol and a dual insertion method would be required. The reason for producing larger actuator based robots is to maintain the ability to perform a successful surgery as a proof of concept and a scientific platform.

Each arm of the desired surgical robot would consist of a “forearm,” “upper arm” and “torso” and would be a mirror of the opposing arm as described by Wortman et al.

[29]. The robot used for the experiment has been deemed TB2.0 prior to enhancements and alterations and features two 4-degree-of-freedom (4-DOF) arms with a cautery and a grasper as the end effectors. As this suitable robotic platform has been identified, it will be used for modification and measurement in an attempt to optimize the design of future *in vivo* surgical robots.

2.5. Measurement Methods

3.1.3. Multi-axis Sensor Selection

Given that TB2.0 was specifically designed as a platform for general use and improvements, it was not difficult to modify it to include a 6-DOF force and torque sensor. The sensor was decided upon based on the size and environment issues as well as previously predicted forces and torques it may encounter. The sensor had to have a small diameter such that it would not interfere with the mechanical abilities of the robot while maintaining the workspace and measurement abilities.

The forces and torques that are given by a device known as the BlueDRAGON by researchers at the University of Washington BioRobotics Lab were originally used as the design requirements for TB2.0. Given that these were the requirements for the platform, the values were used for selecting the multi-axis force measurement sensor. The data from BlueDRAGON can be found in Table 3.1 [24].

Table 3.1: BlueDRAGON surgical force measurements.

Quantity	Value	Units
Force	F _x	5 (N)
	F _y	5 (N)
	F _z	20 (N)

With the forces that were found through the literature review and the known dimensions of the robot, a quick calculation of the required torques was performed. At that time the sensor that was decided upon is manufactured by ATI Industrial Automation and is designated as their Nano25 IP65/IP68 multi-axis force transducer. The IP designation specifies the environment that the sensor can withstand. Given the nature of surgical procedures the IP68, a fully submersible model, was decided on. It was also possible to have the manufacture calibrate the sensor to withstand various loads, and the chosen calibration data are given in Table 3.2 [30].

Table 3.2. ATI-IA Nano25 Specifications with US-25-25 Calibration.

Calibration	F _x , F _y	F _z	T _x , T _y	T _z
US-25-25	25 lbf	100 lbf	25 lbf-in	25 lbf-in
	Sensing Ranges			
	F _x , F _y	F _z	T _x , T _y	T _z
	1/224 lbf	3/224 lbf	1/160 lbf-in	1/320 lbf-in
	Resolution			

Given the approximations and a few experiences during testing it was better to lean on the side of caution and have the sensor be built at a reasonable size that would not receive damage during a standard procedure.

3.1.4. Utilizing Multi-axis Measurement

The end goal of this research is to take measurements of a robotic surgery from a modified currently usable system. Although a new novel system could be produced, given time and funding constraints a proof of concept was desirable. The adaptation of

the platform should be easily applied and interchangeable with the stock configuration and other future improvements.

Given the design and size of both the robot and the multi-axis sensor it was determined that a reading could be taken from the base of the robot and, through a study of mathematics, be transformed to the robot's end effector. Given the size and shape of the robot a pure dynamic approach to the analysis of the robot would be considered more computationally extensive than a static kinematic approach. Although this assumption can be considered true in regards to momentum of the robot's movements, gravity still plays a role on the sensor's readings even in relatively slow and small movements. Therefore, a study on a quasi-static method will be introduced and presented herein. This method then provides an ability to perform a statistical analysis of a surgical procedure to determine the requirements on future robotic development.

2.6. Design Restraints

3.1.5. Robotic Workspace Preservation

Workspace is generally considered the range and volume in which the robot can successfully reach in order to perform the given operations. The primary concern when adapting a current model of a robot is the preservation of the workspace. This is a very important feature of a surgical robot as it allows for a range of actuation that doesn't require gross repositioning or unnecessary adjustments. It is for these reasons a serious look at the multi-axis system's design was developed for efficiency of workspace.

After trial and error it was determined that the sensor would be placed parallel to the insertion rod of the robot. This would allow for the preservation of the kinematics and

workspace of the original design. Special care was also taken to the space around the sensor to ensure there were no unintentional supports or sensor mis-readings. Further discussion on the original and modified robot will be given in later sections.

Chapter 4 Design and methods

2.7. Tyler-Bot 2.0

Considered to be one of the University of Nebraska Advanced Surgical Robotic Laboratory's most successful surgical robot iterations, Tyler-Bot 2.0 (TB2.0) was a prime candidate for modification and research. This model was designed to have quick actuation, efficient motor positioning, small stature, and interchangeable instruments. Given that the robot was designed as a main platform for surgery it was easily changed and reconfigured to feature the multi-axis force and torque sensor. The simple kinematic design and geometric parameters that were designed into TB2.0 provided for excellent and swift calculation. This was mostly due to its in-line coordinate frames and right angle joint placement.

The calculations for the forward kinematics of TB2.0 are relatively straightforward and well documented as the standard Denavit-Hartenberg (DH) parameter method [31]. The method allows for taking the angular motor positions of the actuators and transforming them into a Cartesian coordinate frame. The coordinate frame is usually given as A relative to B in any linkage of the robot; however, it is standard to give the end effector's position relative to the base frame. The kinematics of TB2.0 is analogous to that of later revisions and will be covered in later sections.

4.1.1. Kinematic Design

One of TB2.0's main features is the efficiency of its kinematics. The robot's physical parameters were motivated by both workspace and the simplicity of this necessary calculation for control and movement. A kinematic model of TB2.0 is shown in Figure 4.1. This figure illustrates the base position $\{0\}$ at the plane of symmetry, $\{1,2\}$

at ideally the same point of the shoulder, {3} at the end of the upper arm and beginning of the forearm, and {4} at the end effector of the robot's arm. This frame configuration is mirrored about the axis of symmetry and applied to the second arm in the same manner [29].

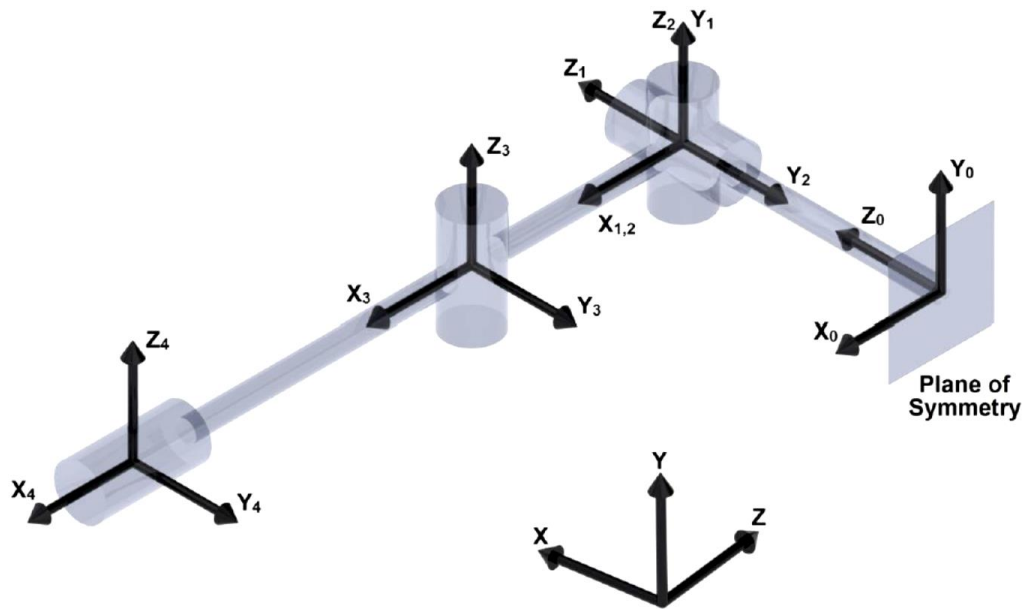


Figure 4.1. Reference frame illustration for TB2.0 [29]

4.1.2. TB2.0 Denavit-Hartenberg Parameters

A standard method for describing a robotic system is known as the Denavit-Hartenberg (DH) parameters. The DH parameters for TB2.0 are presented in Table 4.1. The original configuration of TB2.0 is described by L_1 , L_3 , and L_4 as constant link lengths. L_1 represents the torso length equal to 61.9 mm. L_3 is associated with the length of the upper arm at 50.8 mm. L_4 is the forearm length at 81.4 mm. $(\theta_1, \theta_2, \theta_3, \theta_4)$ define the shoulder pitch and yaw, elbow yaw, and end effector rotation respectively. L_2 is

considered zero as the design intends on the two frames to be at the same point. Each joint limit is also detailed in Table 4.1 [29].

Table 4.1. TB2.0 DH Parameters and joint limits.

i	α_{i-1}	a_{i-1}	d_i	θ_i	θ Limits
1	0	0	$-L_1$	θ_1	-90° to $+90^\circ$
2	-90°	0	0	θ_2	-45° to $+65^\circ$
3	0	L_3	0	θ_3	0° to $+125^\circ$
4	0	L_4	0	θ_4	-180° to $+180^\circ$

4.1.3. Workspace

Workspace can be described as the reachable extent and volume of the robotic arm's end effector. This an essential metric for robotics as it describes the reach and utility a stationary robot can achieve. It is usually found via a study of the minima and maxima X, Y, and Z coordinates using forward kinematics for the full range of joint parameters. Each arm of the surgical robot features an individual workspace and the intersection of the two represents the most usability and utility.

Figure 4.2 illustrates the intersection of the workspace transposed and rotated about a scale model of the large intestine for TB2.0. The side and top views of Figure 4.2 show the workspace for one orientation of TB2.0 while the third image is a color representation of the possible workspaces of TB2.0 when rotated about the main insertion rod. The benefit of a large workspace cannot be stressed enough as many surgical procedures can require access to much of the abdominal region.

The workspace is described by Wortman as “...essentially a 95 mm square revolved around the torso of the robot.” The robot also features a minimum reach of 50.8 mm and a maximum of 132.2 mm. [29]

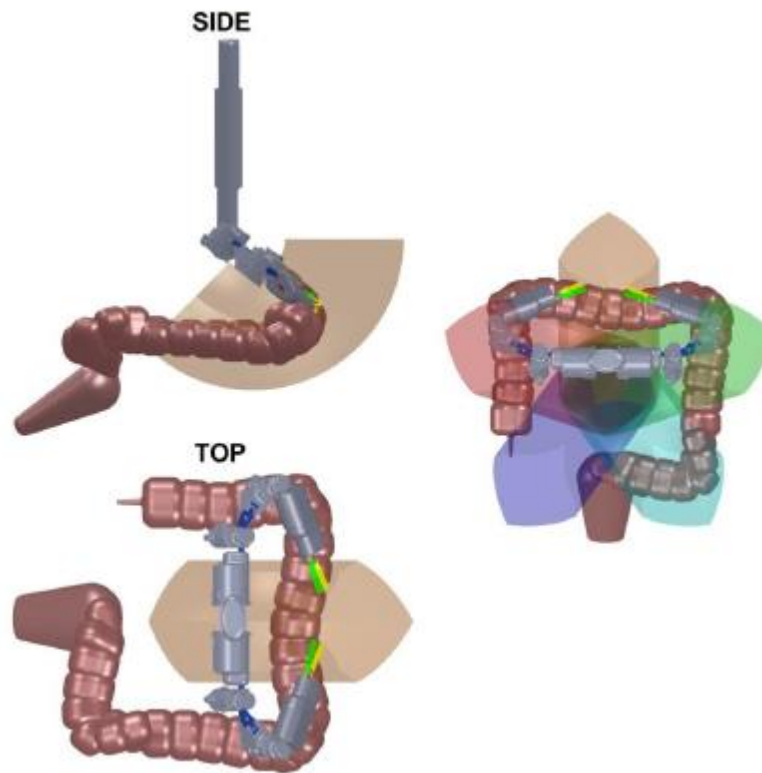


Figure 4.2. TB2.0 workspace modeled beside human large intestine. [29]

4.1.4. Final Design

TB2.0 covers many of the design requirements needed for a LESS procedure in a compact package. Its compact and modular design enables it to be inserted into an impressive 4 mm single site incision. This is primarily achieved by partially disassembling the two arms of the robot and inserting each one separately by a specific procedure. The robot is then reassembled using a control/assembly rod and made secure.

Figure 4.3 gives the computer rendition of TB2.0 to better illustrate the assembly rod configuration.

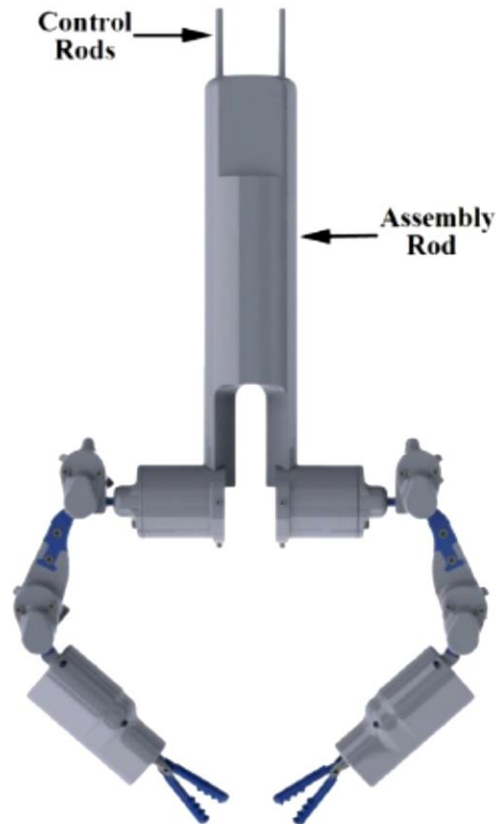


Figure 4.3. Illustration of TB2.0. [29]

In order to protect the robot's electrical components from the moist environment of an *in vivo* surgery, the drive train was encased in a plastic shell. The entire system consists of five motors for actuation that feature small size and encoding abilities. The specific drive train is shown in Figure 4.4.

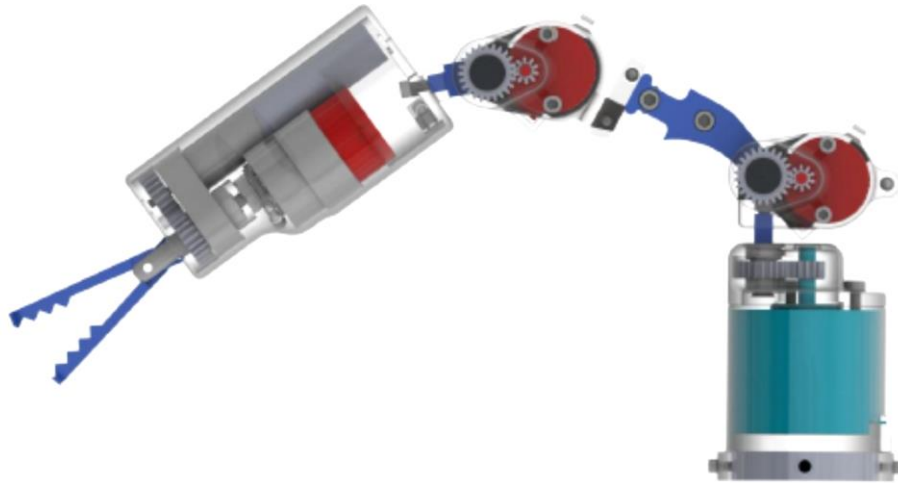


Figure 4.4. TB2.0 Drive train. [29]

The method of the robot's actuation can be found in Figure 4.5 and shows the rotation of each joint. The shoulder of the robot features a 2-DOF joint that gives the arm its pitch and yaw abilities. The upper arm also features 1-DOF yaw movement and gives the robot increased dexterity. Lastly, the end effector has a two-motor system that provides tool rotation and grasper open and close actuation depending on the configuration. The system allows for an effective 4-DOF manipulation which provides dexterity to perform most abdominal procedures.



Figure 4.5. TB2.0's available degrees of freedom. [29]

The final configuration and full assembly of TB2.0 can be found in Figure 4.6. It is from this platform that the remainder of modification and design will be performed. This configuration shows the robot prior to the spacing added for the camera in the insertion rod. While this decreases the footprint of the overall robot it prevents other tools from being used in the LESS procedure. In previously pictured versions of the robot the insertion rod features a small gap that will be used for the multi-axis force sensor.



Figure 4.6. TB2.0 configuration prior to modification. [29]

2.8. Jacob-Tyler-Bot 1.0

Jacob-Tyler-Bot 1.0 was the first design that attempted to incorporate the multi-axis force and torque sensor into TB2.0. The design took features and specifications from the sensor manufacturer and the technical drawings of TB2.0 and merged the two together to create a basic prototype. A side view of the sensor can be found in Figure 4.7 showing the mounting adapter locations. The locations featured three tapped holes for attachment as well as two slots to ensure alignment.

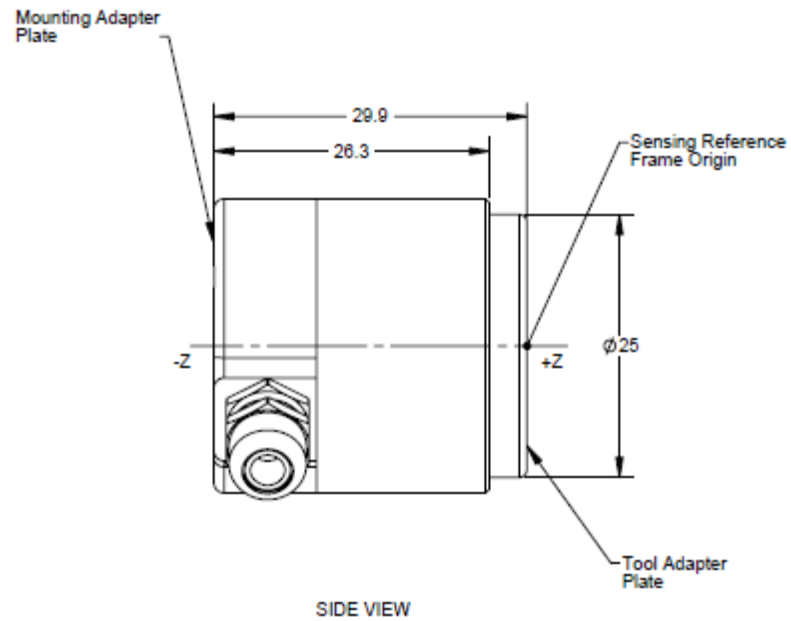


Figure 4.7. Side view of the ATI-ia multi-axis sensor. [30]

In order to interface with the robot it was necessary to create a mounting plate that would fit both the sensor and the robot's current configuration. JTB1.0 attempted to do this by using the minimum amount of modification to TB2.0. It was found that a simple addition of two mounting plates would be sufficient to secure the sensor in series with TB2.0's torso. This was achieved with the plate given in Figure 4.8. The design of the mount would prove to be very versatile in future renditions of JTB thanks to its compact and general design.

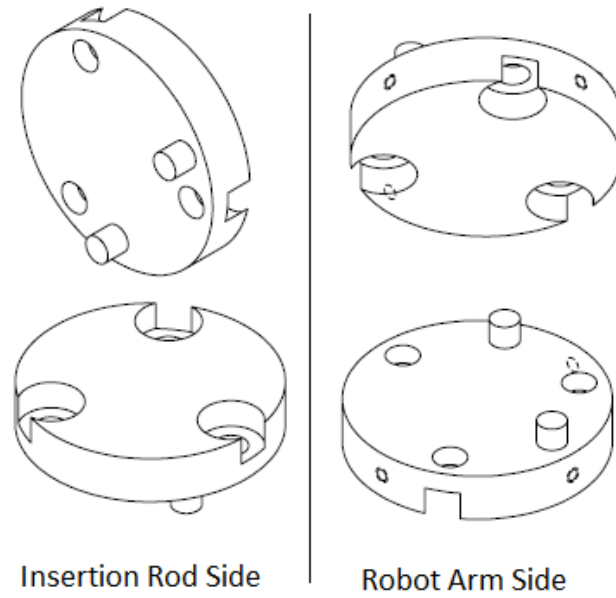


Figure 4.8. Metal mount that converts TB2.0 to the sensor based JTB1.0.

The configuration shown in Figure 4.9 allowed for testing and proof of concept on the left arm of the robot.

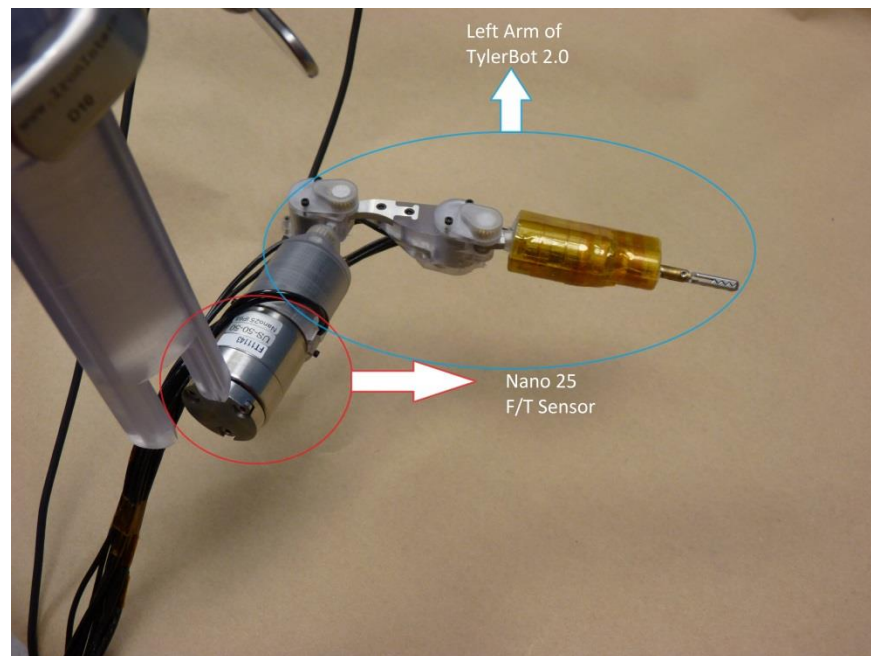


Figure 4.9. Assembled left arm of the JTB1.0 prototype.

The prototype provided good insight into the way the sensor would mount and work but had drawbacks. For one thing the method of attachment extended the left arm's torso which in turn decreased the available intersecting workspace. Therefore this design was never used outside of limited benchtop testing and qualitative examination.

2.9. Jacob-Tyler-Bot 2.0

Given the drawbacks presented by extending the torso in a serial linkage it was necessary to revisit the design of the modifications. The prior system was done in a serial manner that is consistent with conventional robotic systems and recommendations. However, upon further analysis and thought it was discovered possible to put the sensor in a parallel orientation with respect to the insertion rod. This configuration rotated the multi-axis sensor into a position perpendicular to the torso of the robot and allowed for workspace preservation. The new configuration of JTB2.0 is shown in Figure 4.10.

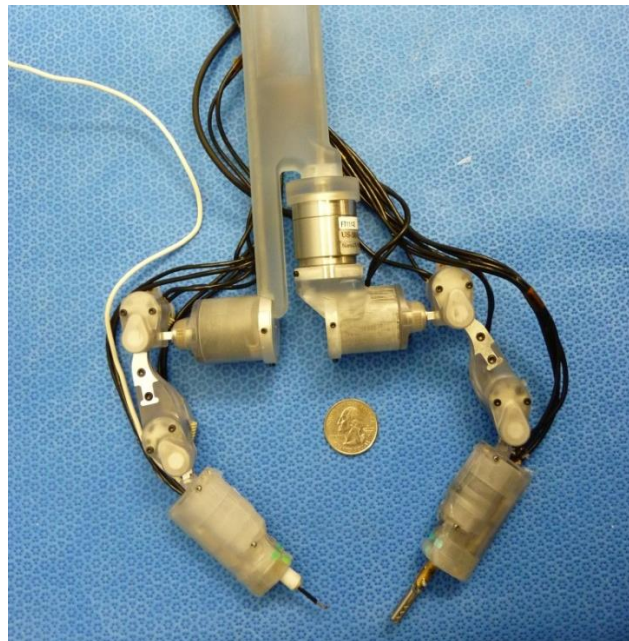


Figure 4.10. JTB2.0 featuring a sensor parallel to the insertion rod.

The design of the system consisted of using one of the previously designed mounting plates from JTB1.0 and the creation of three new pieces of custom plastic. The plastic parts consist of a new insertion control rod, a cup interface, and a new torso casing. These parts were made to specifically fit the multi-axis sensor firmly in place while allowing for no incidental interference and a consistent workspace. The first modification, as pictured in Figure 4.11, enhances the support of each of the TB2.0 arms by bulking up the flanges at the bottom of the rod. It also features a square female port to allow for the sensor to remain rigid and fully supported.

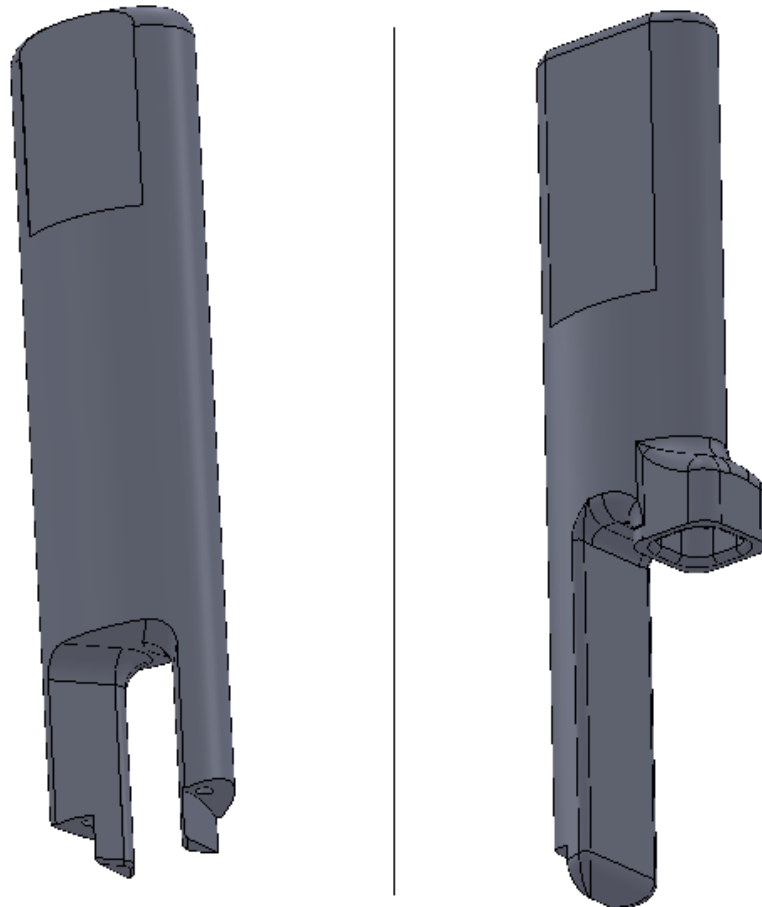


Figure 4.11. Left, TB2.0's original assembly rod; Right, JTB2.0's modified assembly rod.

The next linkage in the system allowed for the insertion rod to interface with the sensor via the aforementioned square female port. The cup interface found in Figure 4.12 was designed to give the orientation of the sensor at just a glance with the -X and +Y axes shown. It attaches and cups the sensor by three bolts with a side slot made to accommodate wiring and alignment. The part also features a square male attachment on the top that sockets into the female port of the insertion rod; this looks to provide rigid and accurate alignment for the sensor.

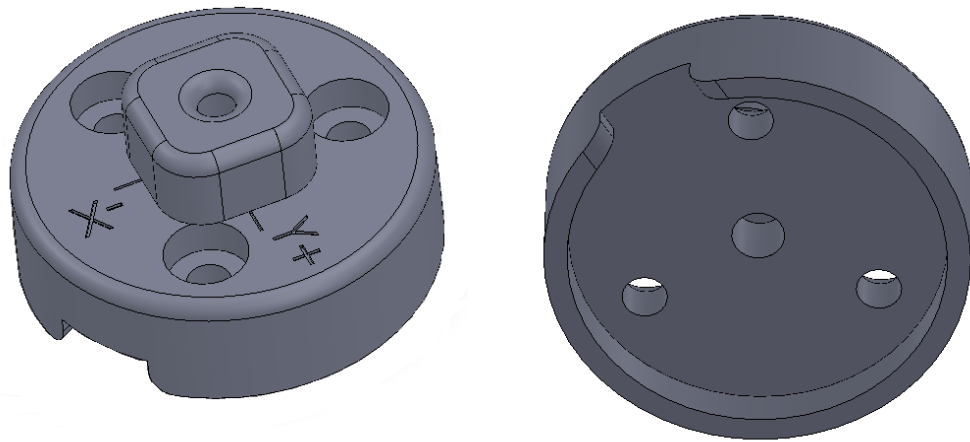


Figure 4.12. Cup interface between multi-axis sensor and insertion rod.

The final modification to TB2.0 that makes the move to JTB2.0 final is the redesigned torso housing. The part, pictured in Figure 4.13, is entirely plastic and allows for an interface between the sensor and the torso. This interface is facilitated by the use of the metal mounting disk designed in JTB1.0 and pictured in Figure 4.8. The use of the previously designed mounting disk was necessary to interface the two, make it rigid, and ease assembly.

The part also provides some of the same features as the cup interface in that it allows for quick visual inspection of the orientation of the sensor. This is shown as the $-Y$ and $+Z$ axis etched onto the surface of the casing. Further enhancements on the original design were to bulk up areas where stress concentrations were identified and to improve wire management.

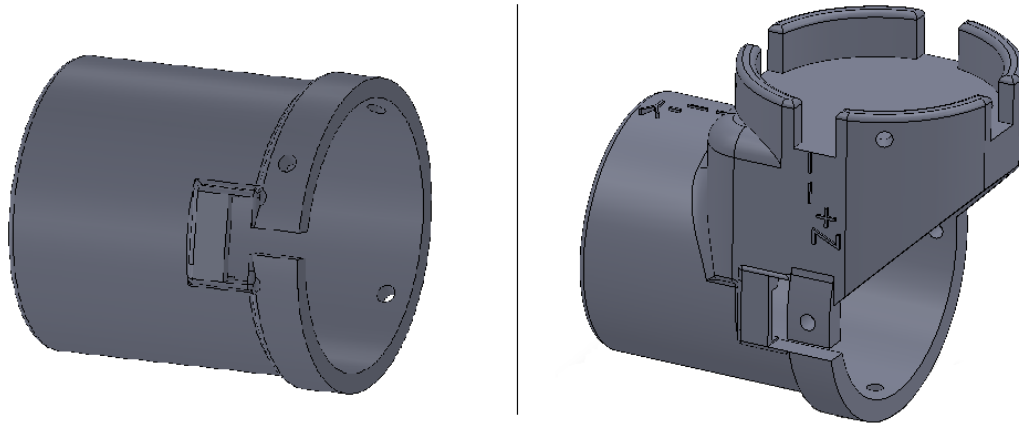


Figure 4.13. Left, original torso housing; Right, modified torso housing.

The completed assembly is illustrated in Figure 4.14. The figure depicts JTB2.0 in its pre-surgical calibration and training setting. At first glance it appears as though it is a more bulky rendition of TB2.0; however, with further investigation it becomes apparent that it differs at the base of the grasper arm (left arm from robot perspective). The similarities of the two robots are a side effect of the kinematic and workspace preservation. The design modifications were done with ease and the stock look is a testament to the modular abilities of TB2.0.

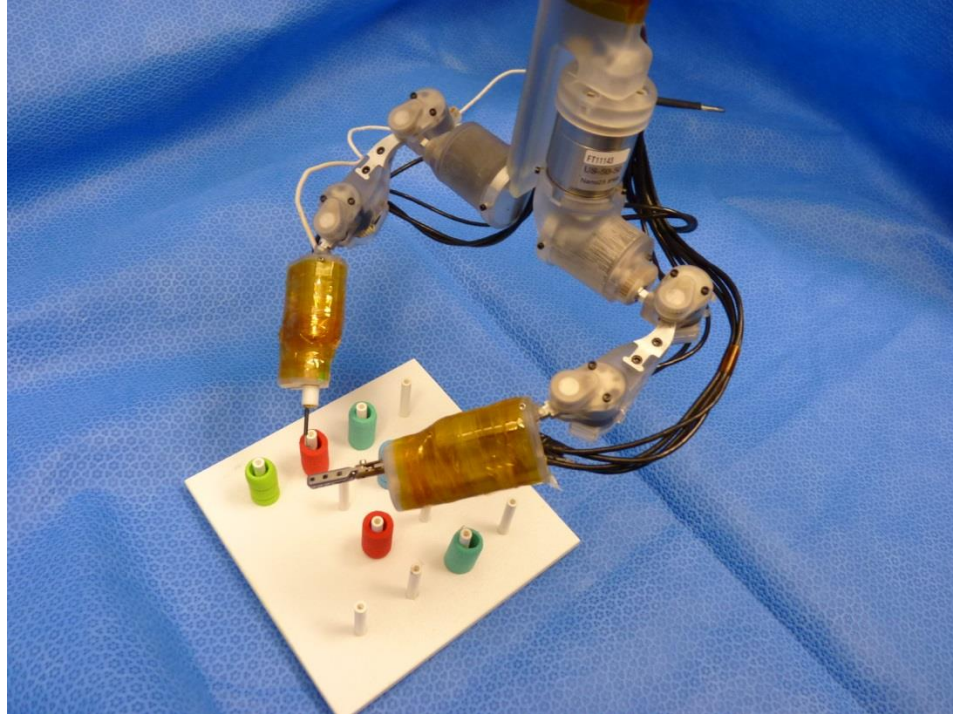


Figure 4.14. Final configuration of JTB2.0.

Once the modifications were completed a simulated model of JTB2.0 was analyzed for a full description of the components' centers of mass and linkage lengths. The results of the simulation findings will be discussed in the following sections.

2.10. Physical Description

Given that the robot was designed with very precise machining and stereo lithography techniques, it was assumed that the computer generated files provided a good reference for link length measurement. The analysis extended further by inserting material properties and average densities of each component into the model, and analyses of the centers of gravity were taken. Although the momentum of each link is neglected, the mass of each is considered important to the quasi-static analysis.

4.1.5. System Coordinate Frames

Each component was modeled in a 3D CAD simulation and reference frames were created at the ends of each link to measure exact values for the Denavit-Hartenberg (DH) Parameters. The values presented by TB2.0 were taken under certain design assumptions, such as: link linearity, absolute coordinate frame alignment, etc. In order to confirm the parameters and provide a more accurate model it was felt necessary to do the CAD analysis and simulation. Pictured in Figure 4.15 is a side by side comparison of the 3D model with the constructed arm. Each of the links was separated in the model and the distances from each joint to the next were measured.

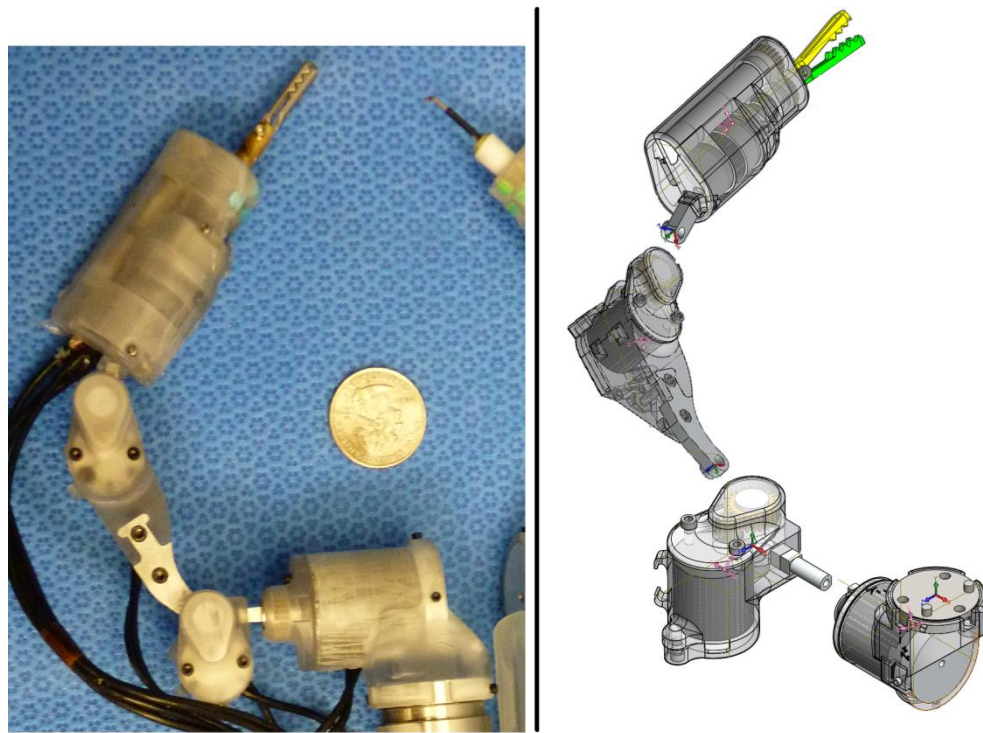


Figure 4.15. Side by side comparison of actual and simulated robot.

A new coordinate frame system was also introduced and is illustrated in Figure 4.16. The new model redefines the DH parameters and sets the system up for a more complete analysis. It is necessary to do this in order to include the base frame rotations caused by the addition of the multi-axis sensor in the analysis. The addition mostly adds an extra element during calculation to rotate the system by standard transformations.

The resulting system features frame $\{0\}$ as the base frame located at the body where the multi-axis sensor is. Between frame $\{0\}$ and frames $\{1, 2\}$ is a intermediate frame in place to break the plane of the system, a necessity to access the sensor. Frames $\{1, 2\}$ are found at the shoulder of the arm and represent 2 DOF. Frame $\{3\}$ is the location of the elbow between the upper and lower arm providing 1 DOF. The final frame, $\{4\}$, is at the end effector and is purely a representative frame giving location without rotation. The final remaining degrees of freedom are grasper twist and actuation and are not considered part of the sensor analysis.

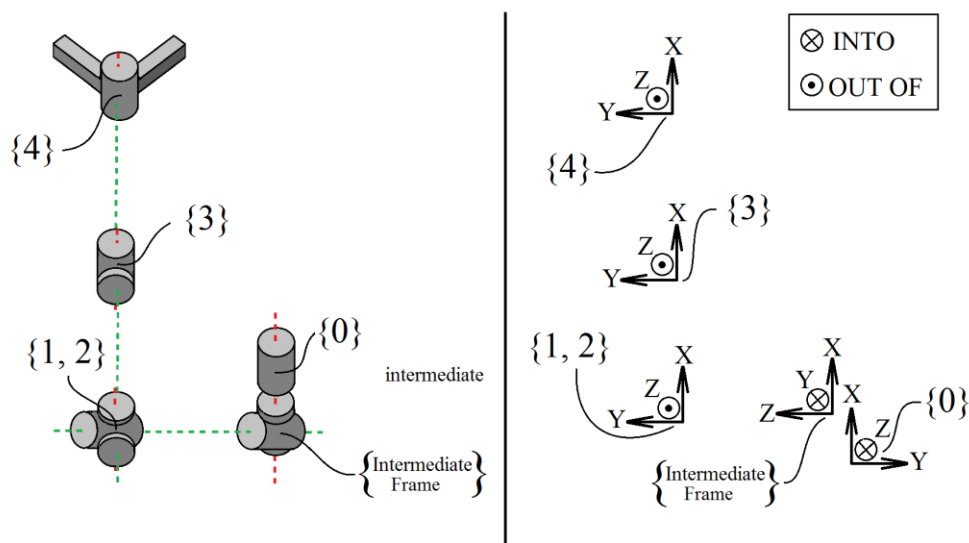


Figure 4.16. New coordinate frame of JTB2.0 in the home position.

4.1.6. JTB2.0 Denavit-Hartenberg Parameters

Utilizing CAD simulation methods Table 4.2 gives the updated DH parameters for JTB2.0 and their comparison to those of TB2.0. The frame numbers transfer from the old system to the new system by allowing for the additional frame to be set at {0}. Furthermore, the addition of {0} is a generalization and allows for a change in orientation of the sensor. A measurement for frame {2} was found but considered to be negligible and retained at zero. Since this study is only interested in the forces and torques acting on at the end effector, the rotation at frame {4} has been omitted in this study.

Table 4.2. Comparison of DH parameters for TB2.0 and JTB2.0.

Frame	α_i		a_i (mm)		d_i (mm)		θ_i		
	new	old	new	old	new	old	new	old	Limits
0	$-\pi/2$	N/A	0	N/A	0	N/A	π	N/A	N/A
1	0	0	8.17 ^(a)	0	50.28 ^(b)	61.9	θ_1	θ_1	-90° to $+90^\circ$
2	$\pi/2$	$-\pi/2$	0	0	0	0	θ_2	θ_2	-45° to $+65^\circ$
3	0	0	49.49	50.8	11.79	0	θ_3	θ_3	0° to $+125^\circ$
4	0	0	69.57 ^(c)	81.4	3.48	0	0 ^(d)	θ_4	-180° to $+180^\circ$

^(a)Value attributed to multi-axis sensor location above TB2.0's original operating plane.

^(b)Value recognized as the shift from the plane of symmetry to center of multi-axis sensor.

^(c)Decrease is seen by the placement of final coordinate from tip of end effector to base.

^(d)The end effector rotation, θ_4 , is removed and no longer necessary.

4.1.7. Gravitational Analysis

To provide a more complete picture of the robotic system during calculation, the gravitational centers of each link were simulated. This was accomplished by applying material properties to each component of the 3D model and running calculations within the software. These calculations took into account material densities and volumes of each link to provide a series of coordinates relative to the joint frame. Figure 4.17 gives an

example of the joint coordinate system and found center of gravity for the upper arm of the robot.

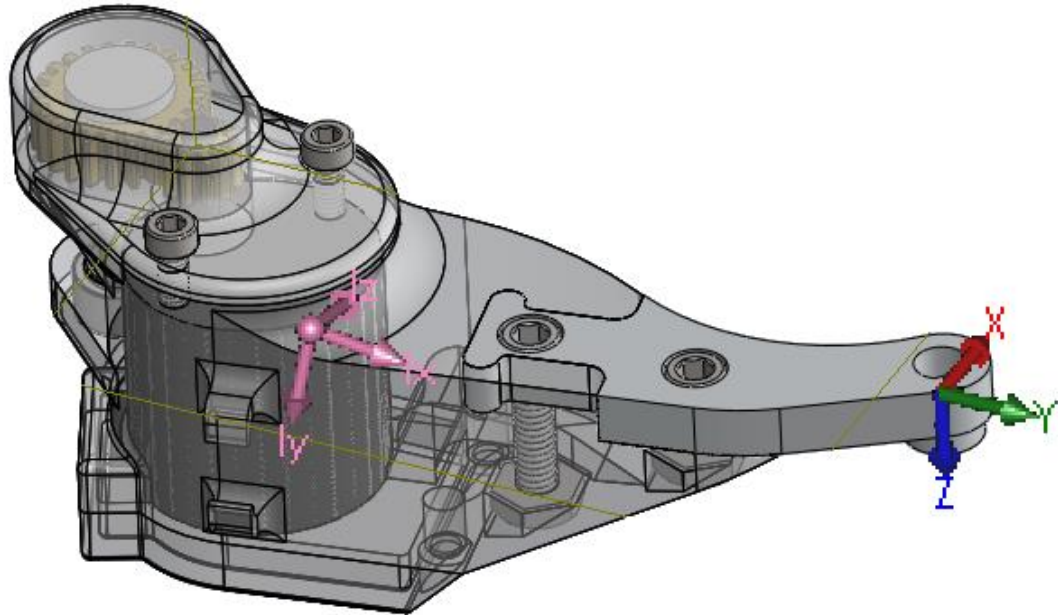


Figure 4.17. Center of mass for the upper arm of JTB2.0.

The resulting coordinates for each center of mass are given in Table 4.3. It is important to note the unit frame orientation in Figure 4.17 differs from the assignment previously given in Figure 4.16. In order to make the information from the simulation useful, it is necessary to transform the simulated link frames into the desired sensor frames. An operation like this is usually performed by treating the frame transitions as right angle Euler rotations and taking the multiplication of each one in descending order ($A = R3 * R2 * R1$). This operation yields a transformation matrix specific to each case.

Table 4.3. Coordinates for the centers of mass.

	Joint Unit Frame				Sensor Unit Frame			
(mm)	0 -> G ₁	1 -> G ₂	2 -> G ₃	3 -> G ₄	0 -> G ₁	1 -> G ₂	2 -> G ₃	3 -> G ₄
X	-10	0.7	-5.1	-10.2	0.05	-8	37.5	37.5
Y	-16.8	-1.1	-37.5	-37.5	-10	-0.7	5.1	10.2
Z	-0.5	8	1.5	4.7	16.8	-1.1	1.5	-4.7

The simulated masses and the associated weight of each link were also found and are given in Table 4.4. Most values for homogeneous components are based upon measurement of the individual components material property data sheets. For heterogeneous structures the mass and dimensions of the item were measured to arrive at density to be used for simulation.

Table 4.4. Simulated mass and weight of each joint of JTB2.0.

Joint	Mass (grams)	Weight ^(a) (N)
1	75.12	0.7369272
2	17.54	0.1720674
3	22.03	0.2161143
4	45.44	0.4457664

^(a)Weight calculated under the gravitational constant, $g = 9.81 \text{ m/s}$.

2.11. Mathematic Derivations

Statics is the study of stable, rigid bodies and systems. Kinematics is the analysis of bodies in motion without consideration for the causes of the motion. Lastly, dynamics is the study of the relationship between moving bodies and their causes. It is usually of

interest to researchers to calculate the most appropriate one of these for the system at hand. However, in the study of robotics, kinematics is mostly used and it is often unnecessary to calculate the dynamics, and statics usually does not apply.

This lack of dynamic analysis is mostly due to the extensive information about the system; simultaneously, static methods are typically disqualified by the active nature of the system. It is the computational complexity of dynamics and the simplicity of static force analysis that motivates a hybrid, quasi-static approach. This approach would make use of a time independent, or instantaneous, view of the system at each moment the sensor is polled.

The method takes the assumption that the small size and slow velocities of the surgical robot make the inertial effects of dynamics negligible. It postulates that the physical robotic system can be considered an infinitely static body at every sensor reading. This quasi-static calculation is made possible by the position and physical description provided by a kinematic solution of the mechanism.

4.1.8. Static Analysis

The quasi-static loading derivation begins with a static analysis of the system given by the generalized free body diagram in Figure 4.18. This diagram gives a description of the interaction between the various links and their associated connections. Each force and moment symbol represents the combined and arbitrary forces and moments on an individual link. The sensor reads the forces and moments at frame $\{0\}$ and the system moves these readings down the successive frames of the robot to the end

effector. Centers of mass are also considered to be of static importance and are captured in the analysis.

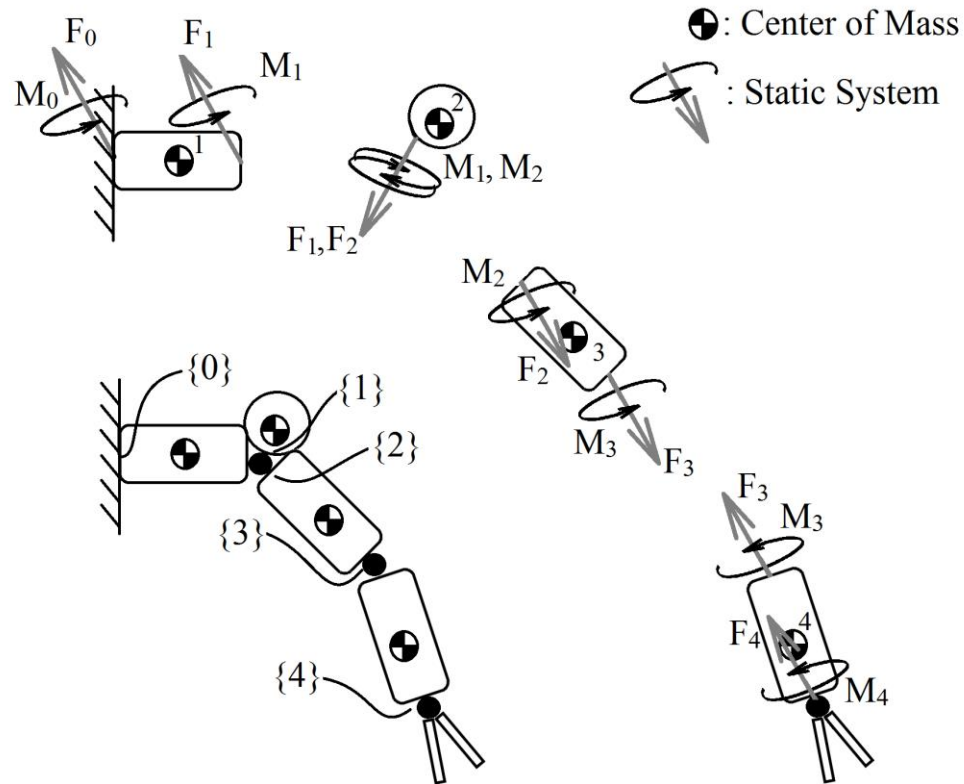


Figure 4.18. Static free body diagram of JTB2.0.

The general assumption that the hybrid solution will be built upon is that the sum of the forces and moments remain zero. These equations are then expanded for each frame giving the force series, Equations 4.1, and the moment series, Equations 4.2. These equations are the sum of forces, F , and the moments, M , with consideration of the centers of mass, G . The forces, both applied and gravitational, move to any point via a couple created from the cross product of their respective orthogonal distance measuring starting position to end position and original vector description. This couple results in an

additional component to the moment applied to each body and can be summed in the traditional sense.

$$\sum F = 0: \quad 4.1.$$

$$\text{Frame 1:} \quad F_1 = F_0 + G_1 \quad 4.1.1.$$

$$\text{Frame 2:} \quad F_2 = F_1 + G_2 \quad 4.1.2.$$

$$\vdots$$

$$\text{Frame } n: \quad F_i = F_{i-1} + G_i \quad 4.1.3$$

The expansion of Equation 4.1 yields the general static force equation for the robot with n frames and is represented as Equation 4.1.3. Similarly, the expansion of Equation 4.2 leads to equation 4.2.3, and is a generalized moment for n frames.

$$\sum M = 0: \quad 4.2.$$

$$\text{Frame 1:} \quad M_1 = M_0 + r_{g,1} \times G_1 + l_1 \times F_0 \quad 4.2.1.$$

$$\text{Frame 2:} \quad M_2 = M_1 + r_{g,2} \times G_2 + l_2 \times F_1 \quad 4.2.2.$$

$$\vdots$$

$$\text{Frame } n: \quad M_i = M_{i-1} + r_{g,i} \times G_i + l_i \times F_{i-1} \quad 4.2.3$$

where r_g is the distance from the center of mass to the end of the current link and l_2 is the length of the link (position of start force to position of end force). These formulas will be used in later derivations to create a hybrid approach.

4.1.9. Kinematic Analysis

The robot is fairly simple to emulate kinematically from the previously mentioned DH parameters. Equation 4.3 gives the standard equations to represent frame i relative to

frame $i-1$. This equation allows for the direct transfer from a DH parameter description to a kinematic description of the required transforms [31].

$${}^{i-1}T_i = \begin{bmatrix} c\theta_i & -s\theta_i & 0 & a_{i-1} \\ s\theta_i c\alpha_{i-1} & c\theta_i c\alpha_{i-1} & -s\alpha_{i-1} & -s\alpha_{i-1}d_i \\ s\theta_i s\alpha_{i-1} & c\theta_i s\alpha_{i-1} & c\alpha_{i-1} & c\alpha_{i-1}d_i \\ 0 & 0 & 0 & 1 \end{bmatrix} \quad 4.3.$$

This is useful and it is usually considered a shortcut method; however, if a more precise method of calculation is desired, the standard rotation and transformation matrices can be used in much the same way. Equation 4.4 is the 3x3 subset of Equation 4.3 that represents the rotations to frame i relative to the $i-1$ frame [31].

$${}^{i-1}R_i = \begin{bmatrix} c\theta_i & -s\theta_i & 0 \\ s\theta_i c\alpha_{i-1} & c\theta_i c\alpha_{i-1} & -s\alpha_{i-1} \\ s\theta_i s\alpha_{i-1} & c\theta_i s\alpha_{i-1} & c\alpha_{i-1} \end{bmatrix} \quad 4.4.$$

If each rotation is considered to be created based upon Euler angles it is then possible to compound them to create a rotation of the complete system giving $\{n\}$ relative to $\{0\}$ as shown in Equation 4.5. This is typically used to gather detailed information on a frame by frame basis.

$${}^nR_0 = {}^nR_{n-1} \dots {}^4R_3 {}^2R_1 {}^1R_0 \quad 4.5.$$

4.1.10. Quasi-Static Derivation

It is from the two methods above that a hybrid approach to the forces involved in the moving robotic system can be made. This approach treats forces as a Cartesian vector that can be rotated by the rotation transform in Equation 4.5 to be expressed in any desired frame. With that it is possible to construct a 6x6 matrix known as the force-

moment transformation as shown in Equation 4.6 [31]. This equation can be considered to consist of separate quadrants that govern varying attributes to the final solution.

$${}_{FM}^n T_0 = \left[\begin{array}{c|c} Q1 & Q2 \\ \hline Q3 & Q4 \end{array} \right] = \left[\begin{array}{c|c} {}^n R_0 & \mathbf{0} \\ \hline {}_e^n P_0 * {}^n R_0 & {}^n R_0 \end{array} \right] \quad 4.6.$$

where

$${}_e^n P_0 = \begin{bmatrix} 0 & -p_z & p_y \\ p_z & 0 & -p_x \\ -p_y & p_x & 0 \end{bmatrix} \quad 4.6.1.$$

The top left quadrant, Q1, of Equation 4.6 is a rotation matrix that brings the force vectors expressed in frame {0} into the {n} frame. The top right quadrant, Q2, is a 3x3 zero matrix that eliminates the effect of moments in the pure force calculation. Bottom left, Q3, is the cross product rotation that considers originating forces into the moment calculation. Lastly, Q4 is a pure rotation of the original moments from {0} to {n}. To further explain Q3, Equation 4.6.1 is the analytical skew-symmetric substitute of the vector cross product and is generated by the (x, y, z) coordinates of the end effector, {n}, relative to the sensor frame, {0}.

The proper application of equation 4.6 is given in equation 4.7. F_0 is found by acquiring the 6x1 force and moment description of the system in frame {0} from the multi-axis sensor. This is multiplied using the dot product with equation 4.6 to yield the quasi-static description of forces in the {n} frame, F_n . This is consistent with the description of quadrants given.

$$F_n = {}_{FM}^n T_0 * F_{act} \quad 4.7.$$

With form,

$$F = [f_x \quad f_y \quad f_z \quad m_x \quad m_y \quad m_z]^T \quad 4.7.1.$$

The static system, F , is described by the static analysis previously mentioned. It follows that the sensor reading, F_{sensor} , includes all internal and external forces in the system. Therefore, the mass generated internal forces must be accounted for as shown in Equation 4.8 resulting in F_{act} .

$$F_{act} = [f_x \quad f_y \quad f_z]^T = F_{sensor} - \sum_{i \geq 0}^n G_i \quad 4.8.$$

Similarly, the internal moments must be accounted for as shown in Equation 4.9.

0r_g is the perpendicular distance from sensor frame to the center of gravity, G_i .

$$M_{act} = [m_x \quad m_y \quad m_z]^T = M_{sensor} - \sum_{i \geq 0}^n {}^0r_{g,i} \times G_i \quad 4.9.$$

Chapter 5 Experiments

2.12. Benchtop Experiments

Several benchtop experiments were performed to verify the functionality of JTB2.0 in its modified state. This consisted of operating the robotic system in a controlled setting and going through a series of tests and verifications that would coincide with the demands of a full surgical procedure.

5.1.1. Alignment Protocol

An alignment protocol was developed in order to ensure the system is reading proper values on the assigned coordinate systems. The protocol outlines items such as: center of mass alignment, joint encoder alignment, and order of device activation.

First, the robot platform is set up with surgical clamping equipment to have the control rod as vertical as possible. This ensures that all the centers of gravity are parallel to a pure unit axis normal to ground. From this position the robot is fully supported by a level platform to ensure no readings. Next, the robot is activated from the home position ensuring the positioning system reads zero at the proper coordinate locations. The robot is arranged to have each joint “fall” into the most solid position. This is due to the fact that there is inherently some backlash involved in the design of the robot’s drive train.

Finally, the robot and sensor are then activated with special attention paid to removing *all* forces on the sensor readings. After activation the robot is then set free of all external supports other than the control rod. It is at this point that an initial calibration “spike” is applied to the sensor to identify when the official readings begin.

Once the system has been fully activated at home it is then mounted above the procedure site with the sensor reading all forces involved during operation. The controls of the platform are unlocked and the trial can commence.

5.1.2. Measurement Verification

Since the system is of new design, a series of validating tests were performed to examine different attributes of the robot and the legitimacy of the sensor readings. The first of these tests was to move the robot into various orientations without applying any external force systems. This provided insight into the accuracy of the simulation and gave a basic analysis of the role that inertia played in the system. The next test was to load the robot with a known mass and move the robot around in various orientations. This was to verify that the readings of the sensor did change with the orientation of the robot and gave some fundamental insight into how the systems forces interacted. The results of these tests will be discussed in later chapters.

2.13. Surgical Trials

The procedure of most interest was a colectomy, or a large intestine (colon) resection. In order to maintain validity of the measurements gathered and their compatibility with human anatomy, two successful non-survival trials on living porcine models were performed. Since this trial looked to only examine the force systems required to lift and operate on the large intestine, an open surgery was used to protect the equipment and give unfettered results. Both the surgical robot and the laparoscope used for optics were held in firmly in place over the site of surgical interest. In this case a laparoscope was positioned over the right shoulder of JTB2.0 to give the surgeon a better

view while avoiding unwanted interference with the multi-axis sensor. The surgical setup can be seen in Figure 5.1 and follows the previously mentioned alignment protocol.

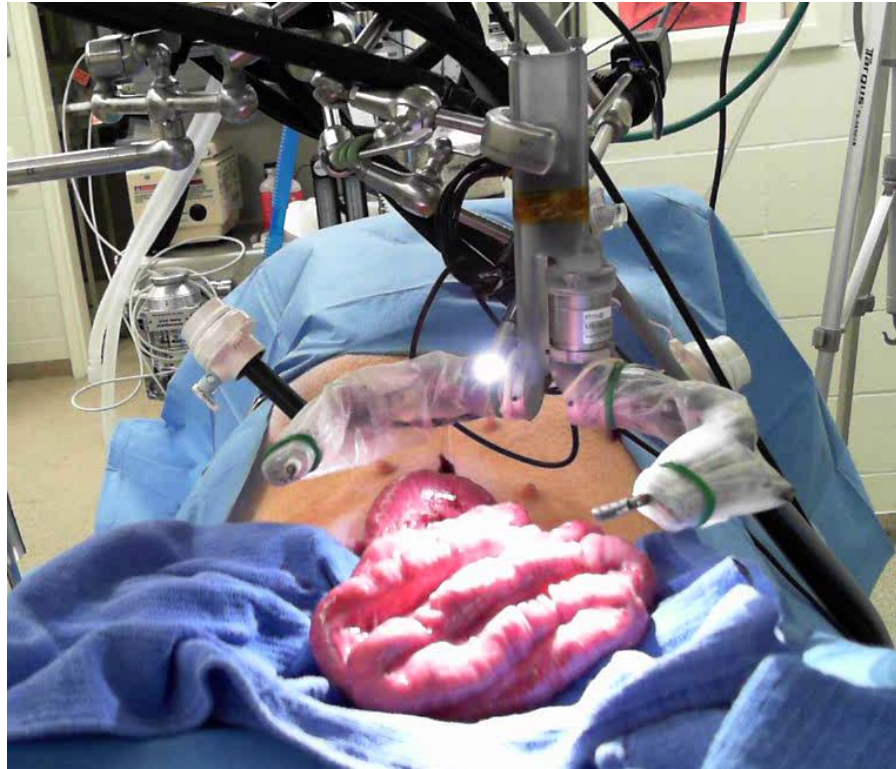


Figure 5.1. Open surgery used to protect equipment.

The primary goal of this trial was to collect force system data on the large intestine to better define design parameters for future surgical instruments. The procedure succeeded in collecting data in the following ways: what is required of the robot to lift the colon, what is required of the robot to stretch the colon between end effectors, and what is the force system needed to perform a supported incision.

Chapter 6 Experimental Results

2.14. Benchtop Experiments

The first controlled experiment was to move the robot without a load as a way to check the validity of the negligible inertia. The raw force and moment data from the sensor are illustrated in Figure 6.1 and Figure 6.2 respectively. In the following text, box and whisker plots will be presented. These can be read as the middle line being the data mean, the edges being first standard deviation, and the whiskers being the second standard deviation.

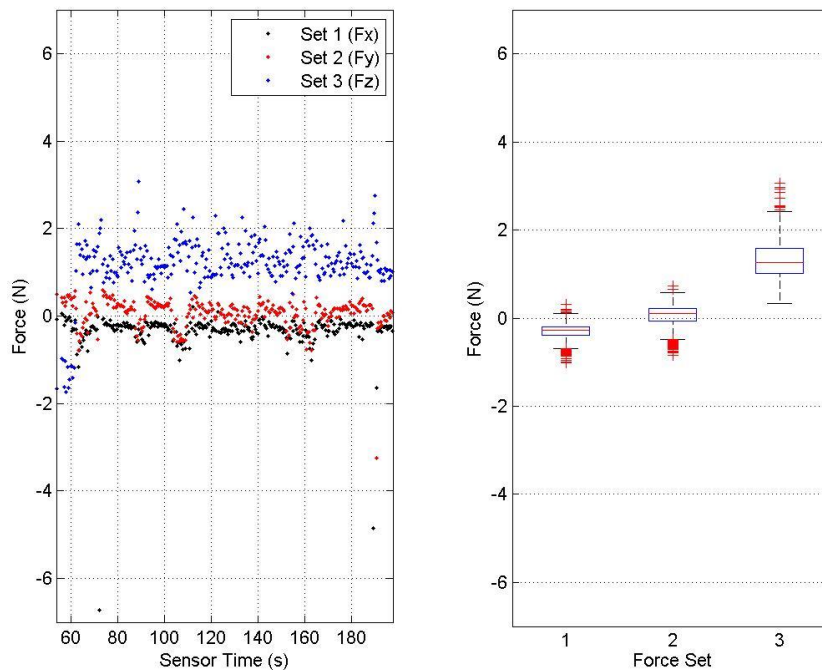


Figure 6.1. Force readings from no load benchtop test.

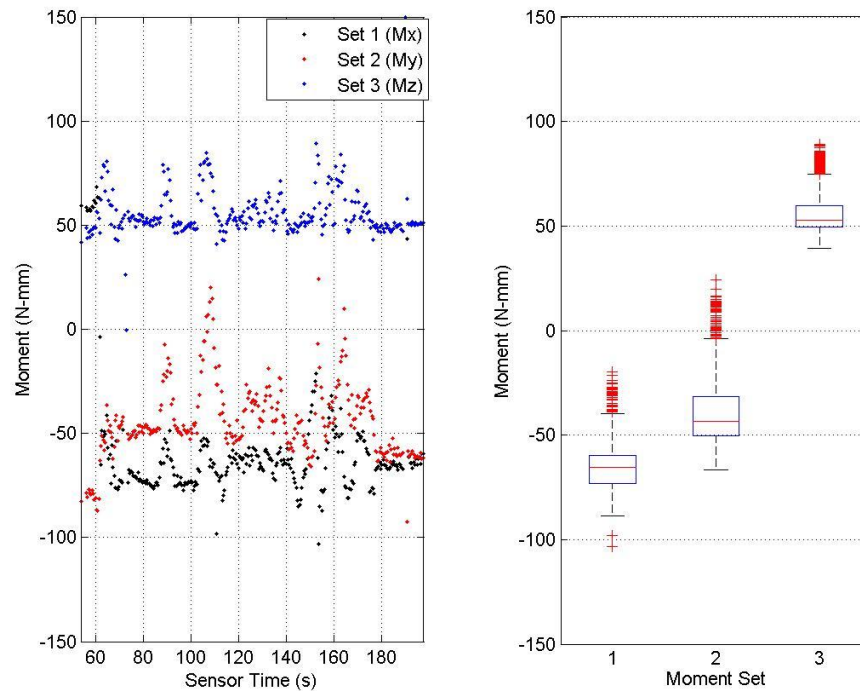


Figure 6.2. Moment readings from no load benchtop test.

The calculated values for mean and standard deviation of the experiment can be found in Table 6.1. Taking the sum of the force values and comparing them to the weights generated by the computer simulation yields a difference of approximately 6.5%; otherwise expressed, the simulated weight was roughly 11 grams lighter than the actual mass reading of the arm.

Table 6.1. Statistical analysis of no load benchtop test.

	Force (N)			Moment (N-mm)		
	X	Y	Z	X	Y	Z
Mean	-0.31	0.05	1.32	-64.75	-39.29	56.02
Standard Deviation	0.17	0.25	0.4	10.99	16.64	9.61

Further experimentation was conducted by putting the arm under load and moving it to set locations. The force and moment data generated in this trial are illustrated in Figure 6.3 and Figure 6.4, respectively. This test provided further verification of the static model given that the forces remained roughly constant despite the arm's position.

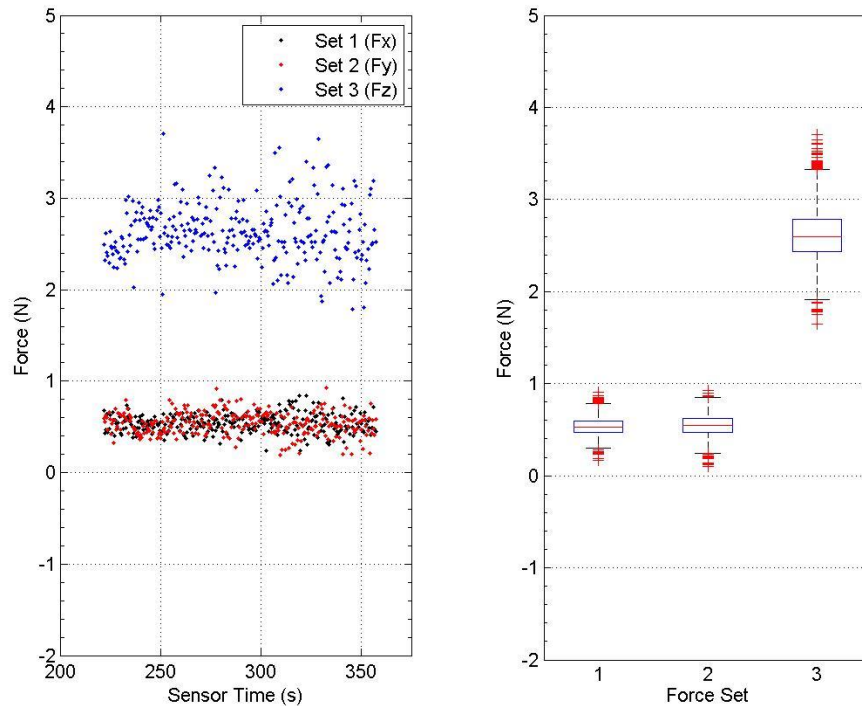


Figure 6.3. Measured forces when moving with a 250 gram load.

The statistical force values of this trial can be found in Table 6.2. By again taking the sum of the three force components it is possible to compare these values to the known applied mass of 250 grams plus the weight of the robot. The comparison with simulated weight would yield a measured 3.71 N and expected value of 4.02 N leading to a difference of 8.3%. Using the measured weight found in the first trial, the expected value

changes to 4.13 N yielding an 11.32% difference. This examination further verified the simulation findings and the multi-axis sensor readings.

Table 6.2. Statistical analysis of forces in trial #2.

	Force (N)		
	X	Y	Z
Mean	0.54	0.55	2.62
Standard Deviation	0.10	0.12	0.31

Quantitatively, the graph of the moments in Figure 6.4 can be read to prove that the moments of the system depend on the position as well as the forces interacting internally and externally.

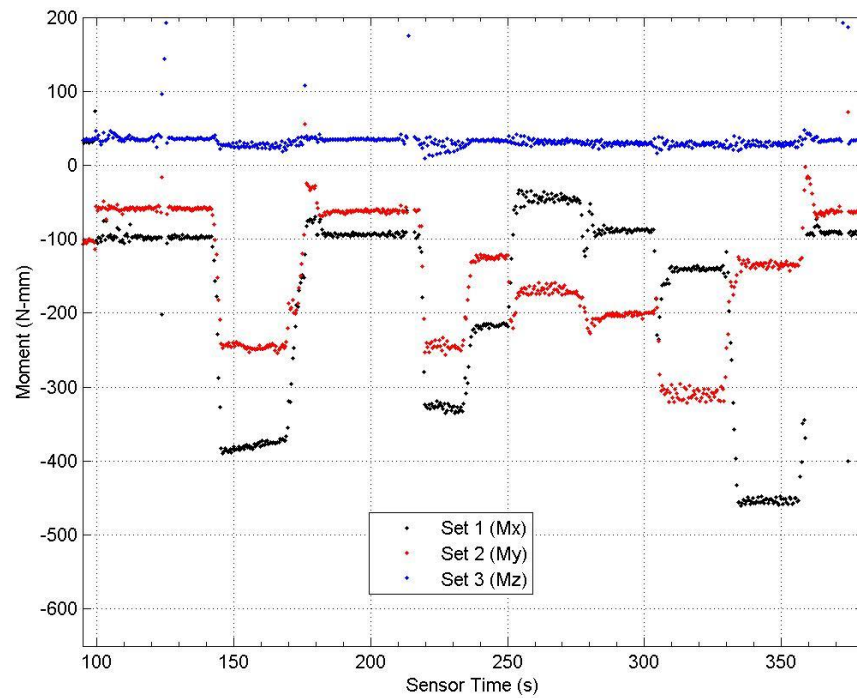


Figure 6.4. Measured moments when moving with 250 gram load.

2.15. Surgical Trial Data and Discussion

The discussed colectomy was performed following the previously outlined alignment protocol. The surgical trial yielded a very worthy raw force data set that can be found in Figure 6.5. It has some very notable features that can be extracted at first glance. For instance, the surgery doesn't begin until around the 500s mark. This is possible to tell due to the alignment protocol causing spikes in the sensor's data at this point. In much the same way the raw moment reading is illustrated in Figure 6.6 and displays promise as well. With these readings it is capable to fully describe the force system of a robotic assisted colectomy with respect to the sensor frame, $\{0\}$, of the surgical robot.

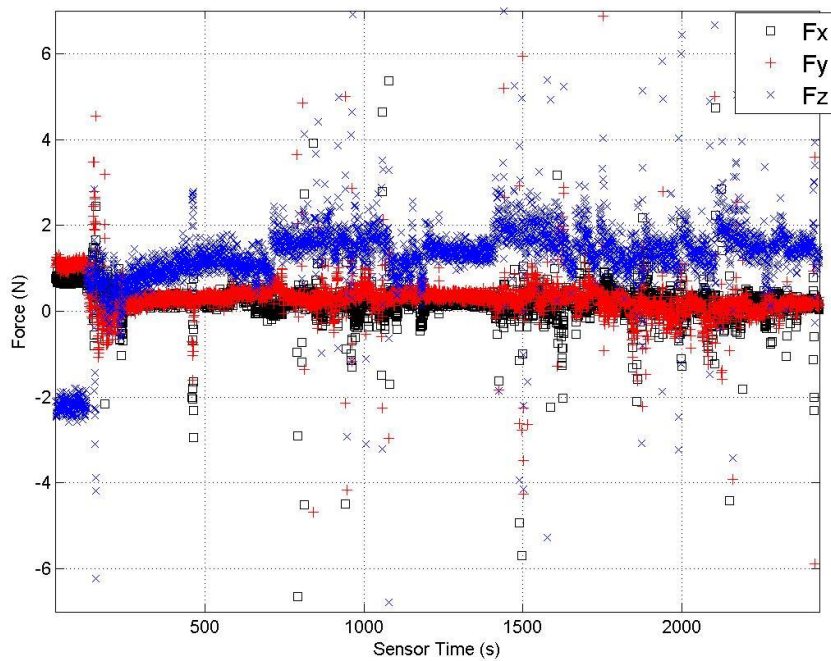


Figure 6.5. Raw surgical force data of a robot assisted colectomy.

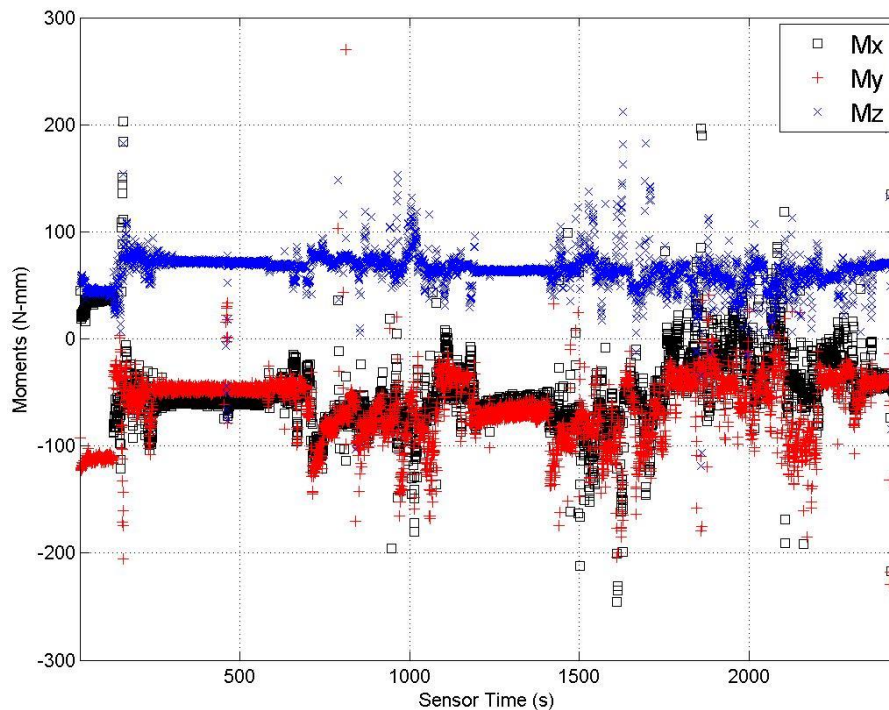


Figure 6.6. Raw surgical moment data of a robot assisted colectomy.

Given that the data presented in Figures 6.5 and 6.6 are in the raw state, it is necessary to trim and align the data to the surgical video. This is done to identify the specific task that the system is undergoing and exactly what force system was felt at that instant. Upon inspection of the alignment points it was found that the data could be trimmed of the excess values.

Further alignment between the video of the procedure and the data collected allows for a specific task to be centered upon. The main task of interest is the lift and stretch of the colon. This is performed when the colon is first lifted and supported by the grasper arm and then stretched by the cautery arm. The three stages of the procedure are given in Figure 6.9. In the first stage a suitable piece of large intestine is selected and grasped by

the sensor arm. The second stage of the procedure is to lift the large intestine and stretch a piece of the large intestine using the opposing arm to perform the incision. Lastly, the surgical site is surveyed for the next procedure.

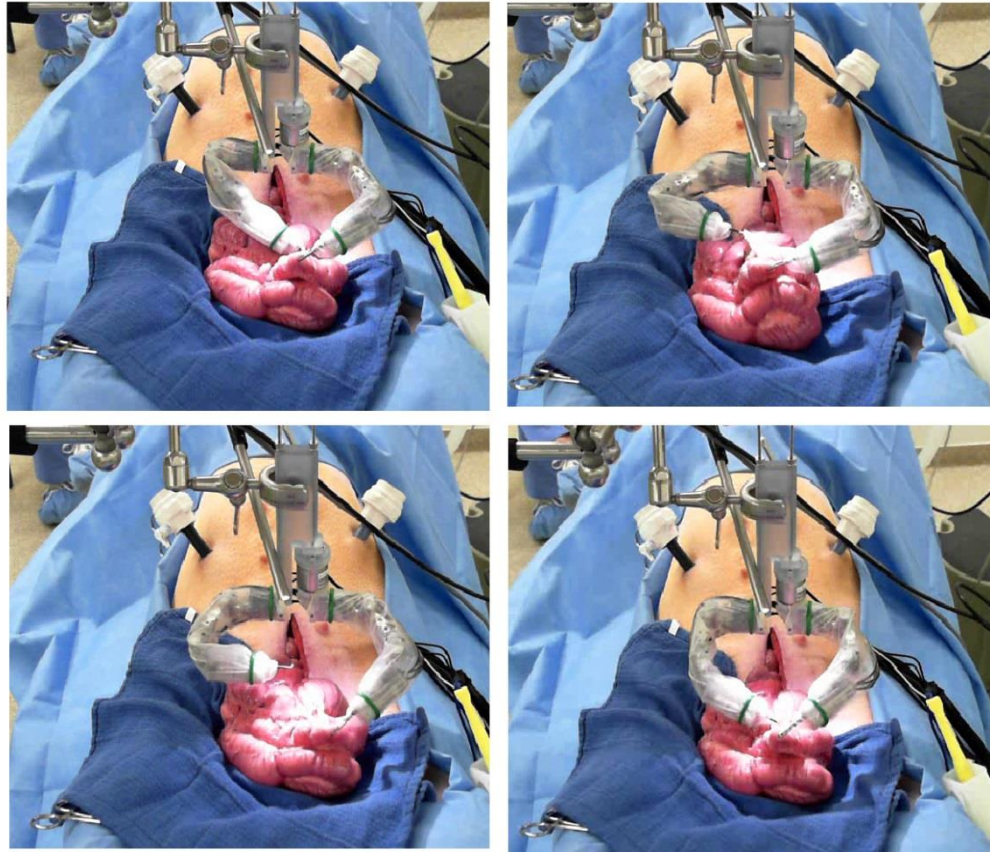


Figure 6.7. Top: left, initial grasp; right, stretching for cut. Bottom: left, arms incision; right, inspection.

The resulting force and moment data acquired from this procedure are then plotted and are illustrated in Figures 6.10 and 6.11 respectively. The forces remain fairly constant as the sensor grasper was used to hold the colon in place while cuts were made. It isn't until about 1576s that the colon is then stretched by the opposing arm and a spike is

created by the snapping action of the tissue suddenly being released. These actions and reactions are congruent to the expected model and match the appropriate sensor frame.

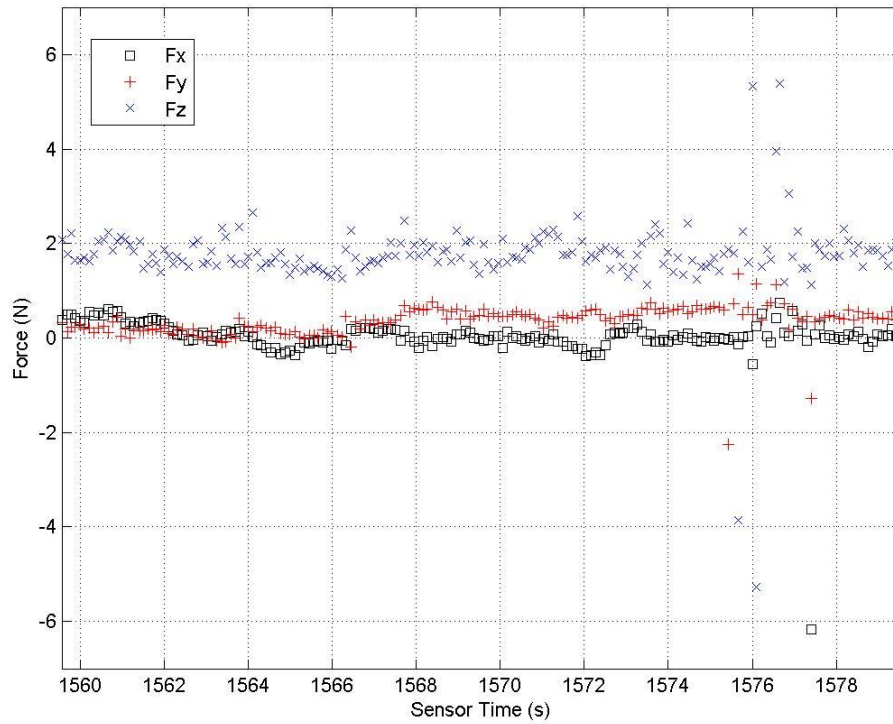


Figure 6.8. Forces measured during a lift and stretch procedure.

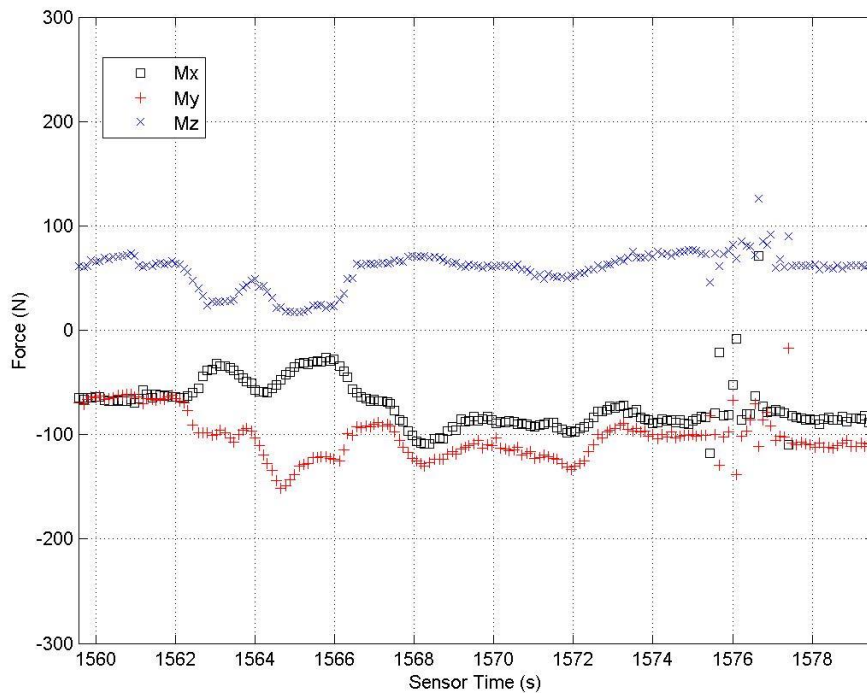


Figure 6.9. Moments measured during a lift and stretch procedure.

The moments given in Figure 6.11 give us a glimpse into how the system is changed by the torque applied to the colon by the robot. The view of the moments is helpful to understanding the complete picture of the force system and can provide insight into when the first disturbances are registered. For instance, the moments begin to register much sooner and more frequently. The detected disturbance here is the cautery arm of the robot performing several cuts, it is important to keep in mind that the forces due to mass are independent of kinematic arm orientation.

2.16. Mathematical Analysis

It is not enough to describe the force system of the colectomy at the base of the robot; to obtain a more detailed understanding of the surgery, it would be more interesting described at the end effector (tool) frame. This is where the hybrid quasi-static loading theory comes into play and gives the best description of the tool frame's force system. This calculation is performed on the selected data subset taking each discrete reading and applying the previously mentioned methods. The results can then be compared to previous surgical findings and design parameters.

At this juncture in the analysis it was time to run the previously presented 20 second data section of the colectomy through the quasi-static loading algorithm. The system successfully transferred the forces from the sensor frame at the shoulder of the robot to the end frame at the wrist. The gratifying result of this analysis can be seen in Figure 6.10 and features a full force map of the quasi-static system. This illustration shows that gravity can successfully be eliminated from the force map via static analysis and the motion of the robot can still be preserved. It also gives insight into the force necessary to support the subsection of large intestine that was operated on during this trial.

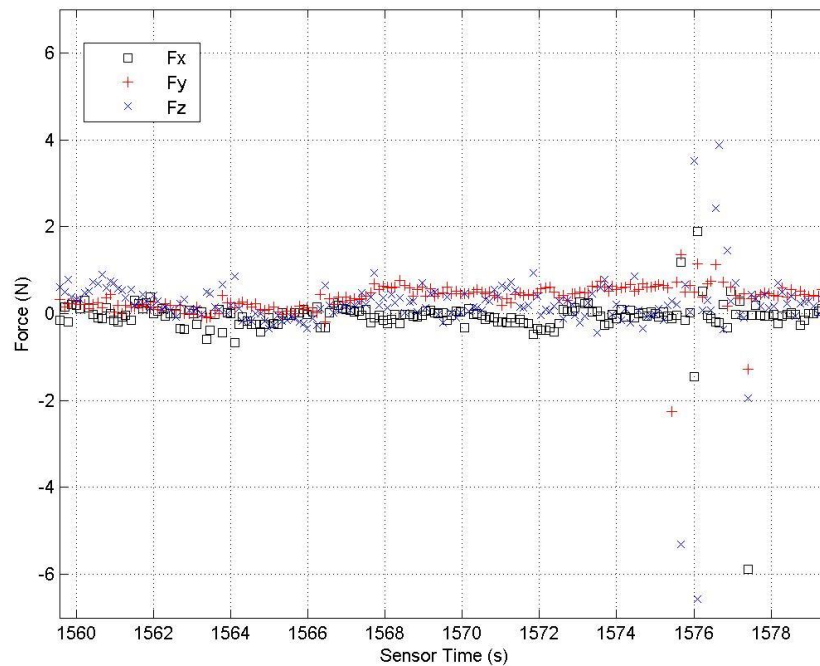


Figure 6.10. Force map after rotation and gravity compensation.

Explaining the interactions in a much more detailed manner, Figure 6.11 presents the moment map of the quasi-static system. Much like the force map, this one has been rotated into the proper end-effector frame and been compensated for moments due to gravity. The small changes in the moments acting at the end effector are most likely due to the pulling and stretching of the colon. In general, this graph gives insight into how much joint torque is required at the end effector in the various coordinate systems. More importantly, the quasi-static system presented here gives more detail into what is required to perform a standard operation.

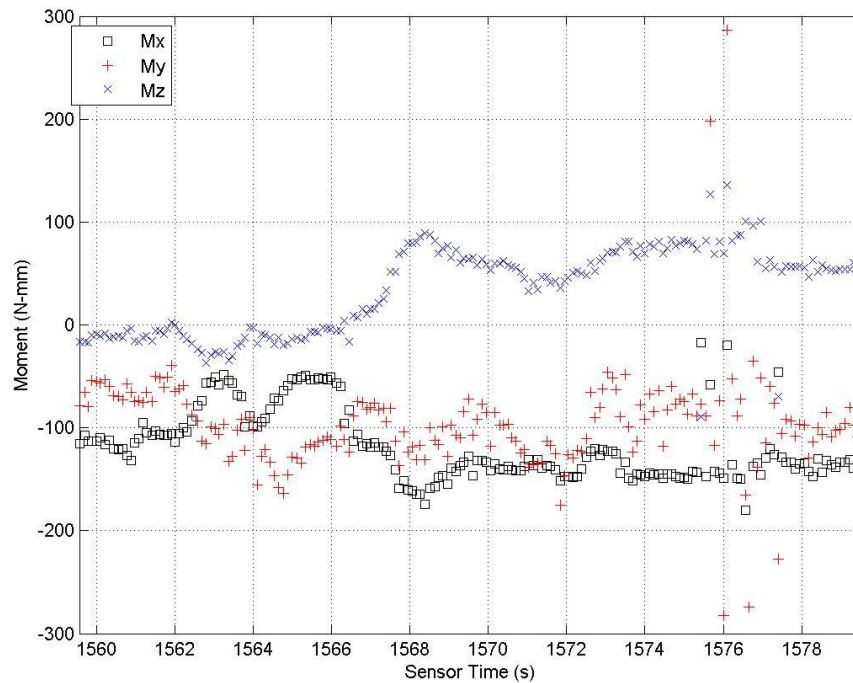


Figure 6.11. Moment map after rotation and gravity compensation.

2.17. Validation

The original parameters that the multi-axis sensor and TB2.0 were designed upon were given by the BlueDRAGON research paper and are restated in Table 6.3 [24]. It is interesting to note that the values obtained during a robot assisted surgery were found to be less than those reported by previous findings. This could be due to the nature of the work that was performed in each study and also the inherent nature of the mechanisms used, but it is uncertain. However, it is important to note that the values that were found are relatively consistent with the research findings in both scale and orientation.

Table 6.3. BlueDRAGON surgical force measurements.

Quantity		Value	Units
Force	F _x	5	(N)
	F _y	5	(N)
	F _z	20	(N)

The findings can further be compared to the original design parameters of TB2.0. This design sought to optimize the utility of the robot in the surgical setting by having a good average force characteristic across the workspace while maintaining a small stature. Originally, TB2.0 was configured to handle forces of 10.3 N, 14.8 N, and 25.5 N in the respective X, Y and Z directions. Although this does add a reasonable factor of safety to the system, future models of surgical robots would have the option of lowering the required workspace operating forces given the historical and newly found data.

In passing, with review of the footage from several surgical trials it may be of interest to perform a further study of other capabilities required by surgical robots. Such capabilities that are assumed to be of most importance, such as average tip velocity, might be worth investigating on a joint by joint basis.

Chapter 7 Summary and Conclusions

As a proposal for a new method of modeling physical systems and an avenue to possible enhancements for design of future surgical robots, this thesis looked to define quasi-static loading as a new tool. Many subtopics were also covered pertaining to current system adaptation, alignment protocols, and quasi-static system definitions. In many ways there has been resounding success in this research; however, other topics warrant more investigation.

Much to the research's success a new system was developed to transform forces in a kinematic system without requiring a complete dynamic solution. Quasi-static loading can be defined as a method to map the static force system to varying link spaces on the robot while maintaining the kinematic description of the system. This has proved to be useful in describing rigid-body force interactions with active gravitational compensation. Furthermore, it has provided a step in finding that surgical robots can be built on a smaller scale with safer guidelines.

Future research topics can delve further into hybrid approaches to analyze the more complex motions of the robot in a straightforward manner. Likewise, this analysis can be used to obtain a larger data set and better statistical analysis of colectomy and other surgical procedures to investigate further surgical minimization.

References

- [1] J. H. Donohue, "Laparoscopic surgical procedures.," Mayo Clinic proceedings Mayo Clinic, vol. 69, pp. 758–762, 1994.
- [2] R. H. Yuan, W. J. Lee, and S. C. Yu, "Mini-laparoscopic cholecystectomy: a cosmetically better, almost scarless procedure.," Journal of laparoendoscopic advanced surgical techniques Part A, vol. 7, pp. 205–211, 1997.
- [3] A. Interlandi, G. F. Panizzolo, and P. Frasson, "Laparoscopic cholecystectomy. A clinical case series," Minerva Chirurgica, vol. 52, pp. 763–766, 1997.
- [4] B. Champagne, J. J. Stulberg, Z. Fan, and C. P. Delaney, "The feasibility of laparoscopic colectomy in urgent and emergent settings.," Surgical Endoscopy, vol. 23, pp. 1791–1796, 2009.
- [5] M. A. Cuesta, F. Berends, and A. A. F. A. Veenhof, "The 'invisible cholecystectomy': A transumbilical laparoscopic operation without a scar.," Surgical Endoscopy, vol. 22, pp. 1211–1213, 2008.
- [6] C. Zornig, H. Mofid, A. Emmermann, M. Alm, H.-A. Von Waldenfels, and C. Felixmüller, "Scarless cholecystectomy with combined transvaginal and transumbilical approach in a series of 20 patients.," Surgical Endoscopy, vol. 22, pp. 1427–1429, 2008.
- [7] P. Roy and A. De, "Transumbilical multiple-port laparoscopic cholecystectomy (TUMP-LC): a prospective analysis of 50 initial patients.," Journal of laparoendoscopic advanced surgical techniques Part A, vol. 20, pp. 211–217, 2010.
- [8] I. Ahmed and P. Paraskeva, "A clinical review of single-incision laparoscopic surgery," The Surgeon, vol. 9, pp. 1–11, 2011.
- [9] D. I. Ramos-Valadez, C. B. Patel, M. Ragupathi, M. B. Bokhari, T. B. Pickron, and E. M. Haas, "Single-incision laparoscopic colectomy: outcomes of an emerging minimally invasive technique.," 2011.
- [10] M. Aurélio De George, M. Rangel, R. W. Noda, and W. Kondo, "Laparoscopic Transumbilical Cholecystectomy: Surgical Technique," JSLS Journal of the Society of Laparoendoscopic Surgeons Society of Laparoendoscopic Surgeons, vol. 13, pp. 536–541, 2009.
- [11] S. Fransen, L. Stassen, and N. Bouvy, "Single incision laparoscopic cholecystectomy: A review on the complications.," Journal of Minimal Access Surgery, vol. 8, pp. 1–5, 2012.
- [12] H.-J. Han, S.-B. Choi, W.-B. Kim, and S.-Y. Choi, "Single-incision multiport laparoscopic cholecystectomy: things to overcome.," Archives of surgery, vol. 146, pp. 68–73, 2011.
- [13] K. M. Love, C. A. Durham, M. P. Meara, A. C. Mays, and C. E. Bower, "Single-incision laparoscopic cholecystectomy: a cost comparison.," Surgical Endoscopy, vol. 25, pp. 1553–1558, 2011.
- [14] Y. Bao, Z.-W. Jiang, L.-F. Xie, F.-T. Liu, and J.-S. Li, "Robotic-assisted laparoscopic colectomy for colon cancer: a report of 13 cases," Zhonghua wei chang wai ke za zhi Chinese journal of gastrointestinal surgery, vol. 14, pp. 327–329, 2011.

- [15] E. Bertani, A. Chiappa, P. Ubiali, B. Fiore, C. Corbellini, M. L. Cossu, A. Minicozzi, and B. Andreoni, "Role of robotic surgery in colorectal resections for cancer.," *Minerva gastroenterologica e dietologica*, vol. 58, pp. 191–200, 2012.
- [16] P. Dario, E. Guglielmelli, and B. Allotta, "Robotics in medicine," *Proceedings of IEEEERSJ International Conference on Intelligent Robots and Systems IROS94*, vol. 2, pp. 739–752 vol.2, 1994.
- [17] P. Dario, E. Guglielmelli, B. Allotta, and M. C. Carrozza, "Robotics for medical applications," *IEEE Robotics Automation Magazine*, vol. 3, pp. 44–56, 1996.
- [18] J. Hance, T. Rockall, and A. Darzi, "Robotics in colorectal surgery.," *Minerva Chirurgica*, vol. 21, pp. 339–343, 2004.
- [19] C. He, S. Wang, and X. Wang, "Design and Analysis of a Portable Reconfigurable Minimally Invasive Surgical Robot," *Advances in Reconfigurable*, 2012.
- [20] D. G. Jayne, P. R. Culmer, J. Barrie, R. Hewson, and A. Neville, "Robotic platforms for general and colorectal surgery.," *Colorectal disease the official journal of the Association of Coloproctology of Great Britain and Ireland*, vol. 13 Suppl 7, pp. 78–82, 2011.
- [21] A. C. Lehman, J. Dumpert, N. A. Wood, L. Redden, A. Q. Visty, S. Farritor, B. Varnell, and D. Oleynikov, "Natural orifice cholecystectomy using a miniature robot.," *Surgical Endoscopy*, vol. 23, pp. 260–266, 2009.
- [22] T. D. Wortman, A. Meyer, O. Dolghi, A. C. Lehman, R. L. McCormick, S. M. Farritor, and D. Oleynikov, "Miniature surgical robot for laparoendoscopic single-incision colectomy.," *Surgical Endoscopy*, vol. 26, pp. 727–31, 2012.
- [23] Ignis. "Wikimedia Commons, File:Laparoscopic Hand Instruments 001 JPN.jpg" Internet: http://commons.wikimedia.org/wiki/File:Laparoscopic_Hand_Instruments_001_JPN.jpg, Sep. 5, 2009 [August 1, 2013].
- [24] J. Rosen, J. D. Brown, L. Chang, M. Barreca, M. Sinanan, and B. Hannaford, "The BlueDRAGON - a system for measuring the kinematics and dynamics of minimally invasive surgical tools in-vivo," *Proceedings 2002 IEEE International Conference on Robotics and Automation Cat No02CH37292*, vol. 2, pp. 1876–1881, 2002.
- [25] K. Ikuta, T. Kato, H. Ooe, and K. Shinohara, "Surgery Recorder System acquiring position/force information of surgical forceps," *2008 World Automation Congress*, 2008.
- [26] H. de Visser, E. a M. Heijnsdijk, J. L. Herder, and P. V Pistecky, "Forces and displacements in colon surgery.," *Surgical endoscopy*, vol. 16, no. 10, pp. 1426–30, Oct. 2002.
- [27] "Dover Medical" Internet: <http://www.dovermed.co.il/da-vinci-si-surgical-system>, [August 1, 2013].
- [28] G. B. Deutsch, S. A. Sathyanarayana, V. Gunabushanam, N. Mishra, E. Rubach, H. Zemon, J. D. S. Klein, and G. Denoto, "Robotic vs. laparoscopic colorectal surgery: an institutional experience.," *Surgical endoscopy*, vol. 26, pp. 956–63, 2012.
- [29] Wortman, Tyler David, "DESIGN, ANALYSIS, AND TESTING OF IN VIVO SURGICAL ROBOTS" M.S. thesis, Dept. Mech. (and Materials) Eng., Univ. of Nebraska., 2011.
- [30] "ATI: Industrial Automation" Internet: <http://www.ati-ia.com/>, [August 1, 2013].

- [31] John J. Craig, Introduction to Robotics: Mechanics and Control, 3rd ed. Upper Saddle River, New Jersey, Prentice Hall, 2004.

Appendix A. Quasi-static scripts.

```

%%%%%%%%%%%%%%%%%%%%%%%%%%%%%%%%%%%%%%%%%%%%%%%%%%%%%%%%%%%%%%%%%%%%%%%%
%%
%Jacob Greenburg
%Master's Thesis
%Aug. 2013
%%%%%%%%%%%%%%%%%%%%%%%%%%%%%%%%%%%%%%%%%%%%%%%%%%%%%%%%%%%%%%%%%%%%%%%%
%%
%
%File Name: 'moving_no_load_graph.m'
%
%Function: Read raw surgical data and plot force and moment graphs
%

close all
clear all

data=xlsread('Benchtop - moving no load.xlsx');

%Forces (N)
Fx = data(2:end, 7);
Fy = data(2:end, 8);
Fz = data(2:end, 9);

%Moments (N*mm)
Mx = data(2:end, 10);
My = data(2:end, 11);
Mz = data(2:end, 12);

%time (s)
time = data(2:end, 13);
idx1 = find(round(time) == 79); %Desired start time
idx2 = find(round(time) == 185); %Desired End time

%Forces
figure(1)
subplot(1,2,1)
grid on
hold on
axis([min(time),max(time),-7,7])
scatter(time(1:5:end),Fx(1:5:end),'.','k')
scatter(time(1:5:end),Fy(1:5:end),'.','r')
scatter(time(1:5:end),Fz(1:5:end),'.','b')

subplot(1,2,2)
boxplot([Fx(idx1(1):idx2(1)), Fy(idx1(1):idx2(1)),
Fz(idx1(1):idx2(1))])

hold off

%Moments
figure(2)

```



```

%%%%%%%%%%%%%%%%%%%%%%%%%%%%%%%%%%%%%%%%%%%%%%%%%%%%%%%%%%%%%%%%%%%%%%%%
%%
%Jacob Greenburg
%Master's Thesis
%Aug. 2013
%%%%%%%%%%%%%%%%%%%%%%%%%%%%%%%%%%%%%%%%%%%%%%%%%%%%%%%%%%%%%%%%%%%%%%%%
%%
%
%File Name: 'Surgery2_ForReal_Quasi.m'
%
%Function: Read raw surgical data and plot force and moment graphs
%rotating the found data from one frame to the next.
%

clear all
close all
clc

data=xlsread('Surgery 1 -Real Deal, Yo!.xlsx');

%Constant gravity and mass
g = 9.81; %m/s^2
pi = 3.14;
cm1 = .075121; cm2 = .017543; cm3 = .022036; cm4 = .04544; %kg

%Forces (N)
Fx = data(2:end, 10);
Fy = data(2:end, 11);
Fz = data(2:end, 12);

%Weight distribution
w1 = (cm1*g); w2 = (cm2*g); w3 = (cm3*g); w4 = (cm4*g); %N
W = [[0;0;w1], [0;0;w2], [0;0;w3], [0;0;w4]];

%Moments (N*mm)
Mx = data(2:end, 13);
My = data(2:end, 14);
Mz = data(2:end, 15);

%sample time (s)
time = data(2:end, 16);

idx1 = find(round(time) == 1560); %start time
idx2 = find(round(time) == 1580); %End Time

%Angular Position
theta1 = 1*((data(:,1))*pi)/180; %72 counts/deg
theta2 = -1*((data(:,2))-32.3)*pi)/180;
theta3 = 1*((data(:,3))-51.26)*pi)/180;

%quasi-static iterations
for i = idx1(1):1:idx2(1)

```

```

%kinematics
T0 = eye(4,4);% [-1 0 0 0; 0 0 -1 0; 0 -1 0 -1; 0 0 0 1];

T1 = [cos(theta1(i)), -sin(theta1(i)), 0, 0; ...
      sin(theta1(i))*cos(-pi/2), ...
      cos(theta1(i))*cos(-pi/2), -sin(-pi/2), -sin(-pi/2)*50.28 ; ...
      sin(theta1(i))*sin(-pi/2), ...
      cos(theta1(i))*sin(-pi/2), cos(-pi/2), cos(-pi/2)*50.28 ; ...
      0, 0, 0, 1];

T2 =[cos(theta2(i)), -sin(theta2(i)), 0, 8.17; ...
      sin(theta2(i))*cos(0), ...
      cos(theta2(i))*cos(0), -sin(0), -sin(0)*0; ...
      sin(theta2(i))*sin(0), ...
      cos(theta2(i))*sin(0), cos(0), cos(0)*0; ...
      0, 0, 0, 1];

T3 =[cos(theta3(i)), -sin(theta3(i)), 0, 0; ...
      sin(theta3(i))*cos(pi/2), ...
      cos(theta3(i))*cos(pi/2), -sin(pi/2), -sin(pi/2)*11.79; ...
      sin(theta3(i))*sin(pi/2), ...
      cos(theta3(i))*sin(pi/2), cos(pi/2), cos(pi/2)*11.79; ...
      0, 0, 0, 1];

T4 = [cos(0), -sin(0), 0, 49.49; ...
      sin(0)*cos(0), cos(0)*cos(0), -sin(0), -sin(0)*3.48; ...
      sin(0)*sin(0), cos(0)*sin(0), cos(0), cos(0)*3.48; ...
      0, 0, 0, 1];

Joint1=T1*T0;
Joint2=T2*T1*T0;
Joint3=T3*T2*T1*T0;
Joint4=T4*T3*T2*T1*T0;

%Joint Positions
X1=Joint1(1,4);
Y1=Joint1(2,4);
Z1=Joint1(3,4);

X2=Joint2(1,4);
Y2=Joint2(2,4);
Z2=Joint2(3,4);

X3=Joint3(1,4);
Y3=Joint3(2,4);
Z3=Joint3(3,4);

X4=Joint4(1,4);
Y4=Joint4(2,4);
Z4=Joint4(3,4);

%Mass centers
GJ1 = [eye(3,3), [0.05; -10; 16.8] ; [0, 0, 0, 1]];
GJ2 = Joint1 * [eye(3,3), [-8; -0.7; -1.1] ; [0, 0, 0, 1]];
GJ3 = Joint2 * [eye(3,3), [37.5; 5.1; 1.5] ; [0, 0, 0, 1]];

```

```

GJ4 = Joint3 * [eye(3,3), [37.5; 10.2; -4.7] ; [0, 0, 0, 1]];

r1 = [GJ1(:,4) GJ2(:,4) GJ3(:,4) GJ4(:,4)];

%static analysis
Frange = [Fx(idx1(1):idx2(1)), ...
          Fy(idx1(1):idx2(1)), ...
          Fz(idx1(1):idx2(1))];

Fsum = [Fx(idx1(1):idx2(1))-sum(W(1,:)), ...
        Fy(idx1(1):idx2(1))-sum(W(2,:)), ...
        Fz(idx1(1):idx2(1))-sum(W(3,:))];

Mgrav = sum([cross(r1(1:3,1),W(:,1)), ...
            cross(r1(1:3,2),W(:,2)), ...
            cross(r1(1:3,3),W(:,3)), ...
            cross(r1(1:3,4),W(:,4))],2);

Mrange = [Mx(idx1(1):idx2(1)), ...
          My(idx1(1):idx2(1)), ...
          Mz(idx1(1):idx2(1))];

Msum = [Mx(idx1(1):idx2(1))-Mgrav(1), ...
        My(idx1(1):idx2(1))-Mgrav(2), ...
        Mz(idx1(1):idx2(1))-Mgrav(3)];

%hybrid analysis
R = Joint4(1:3,1:3);
Z = zeros(3,3);
P05 = [0 -Z4 Y4; Z4 0 -X4; -Y4 X4 0];
TFM = [ R, Z; P05*R, R];

if i == idx1(1)
    j = 1;
else
j = i - idx1(1);
end

Ftip = TFM * [Fsum(j,:)';Msum(j,:)'];

F(j,:) = Ftip';
end

figure(1)
%subplot(1,2,1)
grid on
hold on
axis([time(idx1(1)),time(idx2(1)),-7,7])
scatter(time(idx1(1):1:idx2(1)-1),F(1:1:end,1),'.','k')
scatter(time(idx1(1):1:idx2(1)-1),F(1:1:end,2),'.','r')
scatter(time(idx1(1):1:idx2(1)-1),F(1:1:end,3),'.','b')

figure(2)

```

```
%subplot(1,2,1)
grid on
hold on
axis([time(idx1(1)),time(idx2(1)),-300,300])
scatter(time(idx1(1):1:idx2(1)-1),F(1:1:end,4),'.','k')
scatter(time(idx1(1):1:idx2(1)-1),F(1:1:end,5),'.','r')
scatter(time(idx1(1):1:idx2(1)-1),F(1:1:end,6),'.','b')
```